Invariant-region-preserving WENO schemes for one-dimensional multispecies kinematic flow models

Juan Barajas-Calonge[a], Raimund Bürger[b,d], Pep Mulet[c], Luis Miguel Villada[a,d,*]

[a]*GIMNAP-Departamento de Matemática, Universidad del Bío-Bío, Avenida Collao 1202, Concepción, Chile*
[b]*Departamento de Ingeniería Matemática, Universidad de Concepción, Casilla 160-C, Concepción, Chile*
[c]*Departament de Matemàtiques, Universitat de València, Av. Vicent Andrés Estellés s/n, Burjassot, Spain*
[d]*CI²MA, Universidad de Concepción, Casilla 160-C, Concepción, Chile*

Abstract

Multispecies kinematic flow models are defined by systems of N strongly coupled, nonlinear first-order conservation laws, where the solution is a vector of N partial volume fractions or densities. These models arise in various applications including multiclass vehicular traffic and sedimentation of polydisperse suspensions. The solution vector should take values in a set of physically relevant values (i.e., the components are nonnegative and sum up at most to a given maximum value). It is demonstrated that this set, the so-called invariant region, is preserved by numerical solutions produced by a new family of high-order finite volume numerical schemes adapted to this class of models. To achieve this property, and motivated by [X. Zhang, C.-W. Shu, On maximum-principle-satisfying high order schemes for scalar conservation laws, J. Comput. Phys. 229 (2010) 3091–3120], a pair of linear scaling limiters is applied to a high-order weighted essentially non-oscillatory (WENO) polynomial reconstruction to obtain invariant-region-preserving (IRP) high-order polynomial reconstructions. These reconstructions are combined with a local Lax-Friedrichs (LLF) or Harten-Lax-van Leer (HLL) numerical flux to obtain a high-order numerical scheme for the system of conservation laws. It is proved that this scheme satisfies an IRP property under a suitable Courant-Friedrichs-Lewy (CFL) condition. The theoretical analysis is corroborated with numerical simulations for models of multiclass traffic flow and polydisperse sedimentation.

Keywords: systems of conservation laws, invariant region preserving, high-order accuracy, multispecies kinematic flow models, finite volume scheme, weighted essentially non-oscillatory (WENO) scheme

1. Introduction

1.1. Scope

This work concerns high-order numerical schemes for spatially one-dimensional systems of N first-order nonlinear conservation laws

$$\partial_t \Phi + \partial_x \boldsymbol{f}(\Phi) = \boldsymbol{0}, \quad \Phi = (\phi_1, \ldots, \phi_N)^{\mathrm{T}}, \quad \boldsymbol{f}(\Phi) \coloneqq (f_1(\Phi), \ldots, f_N(\Phi))^{\mathrm{T}};$$
$$f_i(\Phi) \coloneqq \phi_i v_i(\Phi), \quad i = 1, \ldots, N; \quad x \in I \coloneqq [0, L] \subset \mathbb{R}, \quad t > 0, \tag{1.1}$$

where t is time, x is the spatial coordinate, and the solution $\Phi = \Phi(x, t)$ usually denotes a vector of partial concentrations $\phi_1, \ldots, \phi_N$ (volume fractions or densities) of a number N of species. The components of Φ should be nonnegative and sum up at most to some maximum value $\phi_{\max}$ that depends on the physical system under consideration. Consequently, Φ is assumed to take values in the set

$$\mathcal{D}_{\phi_{\max}} \coloneqq \{\Phi = (\phi_1, \ldots, \phi_N)^{\mathrm{T}} \in \mathbb{R}^N : \phi_1 \geq 0, \ldots, \phi_N \geq 0, \; \phi \coloneqq \phi_1 + \cdots + \phi_N \leq \phi_{\max}\}.$$

---

*Corresponding author

Email addresses: juan.barajas2001@alumnos.ubiobio.cl (Juan Barajas-Calonge), rburger@ing-mat.udec.cl (Raimund Bürger), mulet@uv.es (Pep Mulet), lvillada@ubiobio.cl (Luis Miguel Villada)

The model (1.1) is called "kinematic" since it is assumed that the velocities $v_1, \ldots, v_N$ are not determined by additional balance equations but are explicitly given functions of Φ. The system (1.1) is equipped with the initial condition

$$\Phi(x, 0) = \Phi_0(x) \in \mathcal{D}_{\phi_{\max}}, \quad x \in I, \tag{1.2}$$

and either periodic boundary conditions

$$\Phi(0, t) = \Phi(L, t), \quad t > 0 \tag{1.3}$$

or zero-flux boundary conditions

$$\boldsymbol{f}|_{x=0} = \boldsymbol{0}, \quad \boldsymbol{f}|_{x=L} = \boldsymbol{0}, \quad t > 0. \tag{1.4}$$

We assume that there exists a piecewise differentiable function $w = w(\phi)$ such that

$$\sum_{i=1}^{N} \phi_i v_i(\Phi) = w(\phi) \boldsymbol{\kappa}^{\mathrm{T}} \Phi, \quad \text{where } \phi = \phi_1 + \cdots + \phi_N \text{ and } \boldsymbol{\kappa} := (\kappa_1, \ldots, \kappa_N)^{\mathrm{T}}, \tag{1.5}$$

where $\kappa_1 \geq \kappa_2 \geq \cdots \geq \kappa_N > 0$ are parameters and the function w is assumed to satisfy

$$w(\phi) \geq 0 \quad \text{for all } \phi \in [0, \phi_{\max}], \tag{1.6}$$
$$w(\phi_{\max}) = 0, \tag{1.7}$$
$$w'(\phi) \text{ is nondecreasing, i.e., } w'(\phi) \leq w'(\tilde{\phi}) \text{ if } 0 \leq \phi \leq \tilde{\phi} \leq \phi_{\max}. \tag{1.8}$$

Furthermore, we assume that the system (1.1) is hyperbolic on $\mathcal{D}_{\phi_{\max}}$, and if $\lambda_1(\Phi) \geq \lambda_2(\Phi) \geq \cdots \geq \lambda_N(\Phi)$ are the eigenvalues of the Jacobian matrix $\mathcal{J}_f = \mathcal{J}_f(\Phi)$ at $\Phi \in \mathcal{D}_{\phi_{\max}}$, then it is assumed that there exists a piecewise continuous function $\psi(\phi)$ such that

$$\psi(\phi) \boldsymbol{\kappa}^{\mathrm{T}} \Phi \leq \lambda_N(\Phi) \quad \text{and} \quad w'(\phi) \geq \psi(\phi) \quad \text{for all } \Phi \in \mathcal{D}_{\phi_{\max}}. \tag{1.9}$$

The properties (1.5)–(1.9) related to the function $w = w(\phi)$ are necessary to prove the IRP property for first-order numerical schemes.

System of PDEs like (1.1) arise in various applications including multiclass vehicular traffic [1, 2], the sedimentation of polydisperse suspensions [3, 4, 5, 6], or the separation kinetics of a dispersion of two immiscible liquids under the action of gravity [7]. We herein focus on two alternative applications. The first is multiclass vehicular traffic, where we distinguish between N classes of vehicles differing in preferential (freeway) velocities, and consider a closed road of length L so the final model is the initial-boundary value problem (1.1)–(1.3). The second application is sedimentation of a polydisperse suspension of small solid particles dispersed in a viscous fluid, where we distinguish between N size classes (that settle at different velocities and hence segregate), the x-coordinate usually is a vertical one aligned with gravity, and the zero-flux boundary conditions (1.4) are appropriate. Thus, within that application, the initial-boundary value problem (1.1)–(1.2), (1.4) describes settling of a suspension of initial composition Φ_0 in a closed column. In both applications we seek solutions that satisfy an invariant region preservation (IRP) property, namely, we expect that if $\Phi_0(x) \in \mathcal{D}_{\max}$ for all x, then $\Phi(x, t) \in \mathcal{D}_{\max}$ for all x and $t > 0$. (A function $w = w(\phi)$ satisfying (1.5)–(1.9) can easily found for each of the multiclass traffic and polydisperse sedimentation models studied herein.)

In the scalar case $N = 1$, and where the unknown is $\phi = \phi(x, t)$, the governing equation turns into the scalar conservation law $\partial_t \phi + \partial_x f(\phi) = 0$, where $f(\phi) = \phi v(\phi)$ is assumed to be a non-negative Lipschitz continuous function with support in $(0, \phi_{\max})$. The periodic and zero-flux initial-boundary value problems then possess unique entropy solutions $\phi(x, t)$ taking values in $[0, \phi_{\max}]$ for all $t > 0$ provided that $\phi_0(x) \in [0, \phi_{\max}]$ for all $x \in I$. (This is the IRP property in the scalar case.) However, existing high-order numerical schemes for solving these problems do not necessarily yield numerical values in that interval but produce oscillations with slight under- and overshoots. To handle this shortcoming, Zhang and Shu [8] proposed a technique to create high-order schemes that do satisfy the IRP property. For one space dimension, the idea is based on utilizing a standard two-point monotone numerical flux,

which if directly applied to the cell averages of the numerical solution adjacent to a cell interface would generate an IRP scheme of first-order accuracy only. The key idea to ensure high-order accuracy consists in evaluating the numerical flux on high-order reconstructions of the unknown to both sides of the cell interface. These reconstructions are obtained by linear scaling around the cell average of the solution in those neighboring cells in conjunction with a limiter function that controls the extrema of the reconstruction polynomial to ensure that the reconstructed solution values lie within $[0, \phi_{\max}]$ (in our setting). This procedure ensures high-order accuracy in space, and is combined with a strong stability preserving (SSP) Runge-Kutta (RK) time discretization [9, 10] to ensure high-order accuracy in time. The computation of the limiter involves determining the extrema of the reconstruction polynomial on the whole cell; this task is simplified if these extrema are replaced by evaluations of the polynomial on the finite set of nodes of the Legendre-Gauss-Lobatto quadrature formula on each interval.

It is the purpose of the present work to introduce high-order finite volume schemes with the IRP property for the general case ($N \geq 1$) of the initial-boundary value problems (1.1)–(1.3) and (1.1)–(1.2), (1.4). To put the novelty into the proper perspective, we mention that first-order finite volume schemes with the IRP property for at least one of these problems have been studied in [11, 12, 13] while high-order WENO approximations for the same models have been advanced in [14, 15, 16, 17, 18, 19]. However, the IRP property is not ensured a priori by any of these available WENO-based treatments, in which spurious oscillations and negative solution values can be observed in the numerical results. Based on the ideas of [8, 20, 21], we herein construct high-order finite volume numerical schemes for the initial-boundary value problems (1.1)–(1.3) and (1.1)–(1.2), (1.4) that do satisfy the IRP property. In fact, the linear scaling limiter advanced in [8] cannot be applied directly to this class of problems since if we denote by $\phi_{i,j+1/2}^{\mathrm{L,R}}$, $i = 1, \ldots, N$ the reconstructed values at the cell boundaries, and supposedly applied the linear scaling limiter of [8] to ensure that $\phi_{i,j+1/2}^{\mathrm{L,R}} \in [0, \phi_{\max}]$ for $i = 1, \ldots, N$, then it would not be ensured that $\phi_{j+1/2}^{\mathrm{L,R}} := \phi_{1,j+1/2}^{\mathrm{L,R}} + \cdots + \phi_{N,j+1/2}^{\mathrm{L,R}} \leq \phi_{\max}$. Consequently, the corresponding reconstructed solution vector $\Phi_{j+1/2}^{\mathrm{L,R}}$ would not belong to $\mathcal{D}_{\phi_{\max}}$. To solve this issue, that is, to guarantee that

$$\Phi_{j+1/2}^{\mathrm{L,R}} \in \mathcal{D}_{\phi_{\max}} \quad \text{for all } j, \tag{1.10}$$

and to point out the novelty, we herein propose a two-step approach: in the first step, a high-order polynomial reconstruction of each component ϕ_i on each cell is applied to ensure that the reconstructed cell interface values for each species are nonnegative, which is achieved by a modified version of the linear scaling limiter originally proposed in [8]; and in the second step, another linear scaling limiter is applied to the sum of the reconstruction polynomials (those of the first step) to ensure that the final reconstructed concentration values at the cell interfaces sum up to at most to $\phi_{\max}$. It is proven that this procedure ensures that (1.10) holds.

The cell- and species-wise high-order polynomial reconstructions (to which the above-mentioned two-step procedure is applied in each time step) are chosen as central weighted essentially non-oscillatory reconstructions proposed by Levy, Puppo, and Russo in [22]. The advantage of this choice is that the underlying reconstructions do not only provide single point values but a complete spatial reconstruction with adaptive spatial order in every time step, which is beneficial for evaluating the extrema of the reconstruction polynomials in each cell. However, it is possible to use other alternatives such as WENO-JS [23], MR-WENO [24], WENO-Z [25] or WENO-AO [26] reconstructions (with some modifications) in the implementation of the limiters. The numerical flux is chosen as the local Lax-Friedrichs (LLF) or Harten-Lax-van Leer (HLL) numerical flux [27]. For both we prove that, under a suitable CFL condition, the first-order method applied to either initial-boundary value problem has the IRP property. That said, it is possible to utilize alternative numerical fluxes such as the Hilliges-Weidlich (HW) flux [12, 28] for the MCLWR model. As stated above, the fully discrete scheme employs an SSP total variation diminishing (TVD) Runge-Kutta time discretization.

1.2. Related work

Numerical methods preserving physical properties of multiclass models have been explored in several works. For instance, Jaouen and Lagoutière [29] propose a second-order numerical algorithm for the transport of an arbitrary number of materials that is conservative for the mass of each component, i.e., each mass fraction stays in [0, 1] and the sum of all mass fractions does not exceed one. Ancellin et al. [30] advance a volume-of-fluid (VOF) method that guarantees natural properties of the volume fractions of a multi-phase flow. In the same direction, Baumgart and Blanquart [31] propose a simple method for preserving the sum of mass fractions in transport without penalizing the inert species. Recently, Huang and Johnsen [32] proposed a general numerical approach, consisting of a consistent limiter

and the multiphase reduction-consistent formulation, to solve the multiphase Euler/phase-field model for compressible N-phase ($N \geq 1$) flows in a consistent and conservative form. Finally, Bürger et al. [13] proposed a first-order antidiffusive and Lagrangian-remap scheme for the MCLWR traffic model which has the IRP property under certain CFL condition depending on the number of species N. The study of high-order IRP numerical methods is of interest also for other kinds of problems. For instance, one can find schemes preserving density and pressure for the Euler equations of compressible gas dynamics [20, 33, 34] or numerical methods preserving positivity for the shallow water equations [35, 36]. An exhaustive survey of property-preserving numerical schemes for conservation laws and further references are provided in the recent monograph by Kuzmin and Hajduk [37].

1.3. Outline of the paper

The remainder of the paper is organized as follows. The multispecies kinematic flow models studied are described in Section 2, including models of multiclass vehicular traffic (Section 2.1) and polydisperse sedimentation (Section 2.2) along with their respective bounds of the eigenvalues of the Jacobian matrix $\mathcal{J}_f(\Phi)$ of the flux vector $f(\Phi)$. These are obtained with the secular equation (see Appendix A). In what follows, we refer to the particular extension of the LWR traffic model [38, 39] to the multiclass case summarized in Section 2.1 simply as "MCLWR model" and to the model of polydisperse sedimentation in conjunction with the Masliyah-Lockett-Bassoon velocity functions (see Section 2.2) as "MLB model." In Section 3 we first introduce the basic time and space finite volume discretizations (Section 3.1). Then, in Section 3.2 we introduce the first-order LLF method and prove in that it satisfies the invariance of the region $\mathcal{D}_{\phi_{\max}}$ for both MCLWR and MLB models, under a certain CFL condition, while in Section 3.3 we do the same for the HLL method. In Section 4 we briefly describe WENO reconstructions for scalar conservation laws (Section 4.1) and then, in Section 4.2, explain component-wise WENO reconstructions systems of conservation laws. Then, in Section 4.3, which is at the core of the present work, we advance a modification to Zhang and Shu's limiters [8] for multiclass models like (1.1) to ensure that the reconstruction polynomials have the IRP property. Then we consider a G-point Legendre Gauss-Lobatto quadrature formula (for ease of computation of the limiter) and prove that the resulting high-order WENO finite volume scheme is IRP under a CFL condition that depends on one of the quadrature weights. Moreover, in Section 4.4 we adapt the ideas from [20, 40] to rigorously discuss the accuracy of the limiter, with the conclusion that the modification introduced in Section 4.3 does not affect the order of the reconstruction. To obtain the correct order of convergence of the method we use an SSP Runge-Kutta time discretization scheme, see Section 4.5. In Section 5 we present five examples in which the numerical methods introduced in Section 3, together with the invariant region preserving WENO reconstructions of Section 4, are used to numerically solve (1.1) for the MCLWR and MLB models. Finally, in Section 6 we draw some conclusions and discuss open issues.

2. Multispecies kinematic flow models

2.1. Multiclass LWR traffic model

The well-known Lighthill-Whitham-Richards (LWR) kinematic traffic model [38, 39] describes the evolution of the vehicle density $\phi(x, t)$ on a single-lane road by a scalar conservation law $\partial_t \phi + \partial_x(\phi v(\phi)) = 0$, where the velocity function $v = v(\phi)$ is nonnegative and non-increasing ($v' \leq 0$). In [1, 2] this model is generalized to N classes of vehicles with individual densities $\phi_i(x, t)$, $i = 1, \ldots, N$. The governing equations of the resulting multiclass LWR traffic (MCLWR) model are (1.1), where the main assumption specific for the MCLWR model is that

$$v_i(\phi) = \beta_i v(\phi), \quad i = 1, \ldots, N, \quad \beta_1 > \cdots > \beta_N > 0, \quad \phi := \phi_1 + \cdots + \phi_N,$$

that is, drivers of different classes adjust their speed to the total traffic ϕ through the same function $v(\phi)$, and β_i is the free-flowing speed of vehicles of class i on an empty highway. The behavioral law $\phi \mapsto v(\phi)$ may be taken from standard speed-density relations like the Greenshields (GS) model $v(\phi) = 1 - \phi/\phi_{\max}$ [41], where $\phi_{\max}$ represents a maximal car density, or the Dick–Greenberg (DG) model [42, 43]

$$v(\phi) = \min\{1, -C \ln(\phi/\phi_{\max})\} \quad \text{with a constant } C > 0. \tag{2.1}$$

The MCLWR model is strictly hyperbolic whenever $\phi_i > 0$ and $\phi < \phi_{\max}$ [44, 45]. The eigenvalues $\lambda_i(\Phi)$ of the Jacobian matrix of the flux $\mathcal{J}_f(\Phi) := (\partial f_i(\Phi)/\partial \phi_j)_{1 \le i, j \le N}$ satisfy the interlacing property (A.3) with the bounds

$$M_1(\Phi) = \beta_N v(\phi) + v'(\phi)\boldsymbol{\beta}^{\mathrm{T}}\Phi, \quad M_2(\Phi) = \beta_1 v(\phi), \tag{2.2}$$

where $\boldsymbol{\beta} := (\beta_1, \ldots, \beta_N)^{\mathrm{T}}$. We assume that the function $v(\phi)$ has the following properties:

$$v(\phi) > 0 \quad \text{for } 0 \le \phi < \phi_{\max}, \quad v(\phi_{\max}) = 0, \quad v'(\phi) \le 0 \quad \text{for } 0 \le \phi \le \phi_{\max};$$
$$v'(\phi) \text{ is nondecreasing, i.e., } v'(\phi) \le v'(\tilde{\phi}) \text{ if } 0 \le \phi \le \tilde{\phi} \le \phi_{\max}. \tag{2.3}$$

This occurs, for instance, if $v(\phi)$ is chosen according to the DG or GS models. The properties (2.3) ensure that for the MCLWR model

$$M_1(\Phi) < M_2(\Phi) \quad \text{for all } \Phi \in \mathcal{D}_{\phi_{\max}}, \tag{2.4}$$

and it can easily be shown that for the MCLWR model, we may choose $w(\phi) = v(\phi)$ and $\boldsymbol{\kappa} := \boldsymbol{\beta}$ along with $\psi(\phi) = v'(\phi)$ such that (1.5)–(1.9) are satisfied.

2.2. Polydisperse sedimentation

Polydisperse suspensions consist of small solid spherical particles that belong to a number N of species that differ in size or density, and which are dispersed in a viscous fluid. Here we assume that all solid particles have the same density ρ_s and that D_i is the diameter of particle class (species) i, where $D_1 > D_2 > \cdots > D_N$. The sedimentation of such a mixture of given initial concentration $\Phi_0(x)$ in a column of depth L can be then described by the initial-boundary value problem (1.1)–(1.2), (1.4), where ϕ_i denotes the local volume fraction of particle species i. A widely used choice of the velocity functions v_i, which is also supported by experimental evidence, is due to Masliyah [46] and Lockett and Bassoon [47] ("MLB model"). This model arises from the continuity and linear momentum balance equations for the solid species and the fluid through constitutive assumptions and simplifications [4]. For equal-density particles, the MLB velocities $v_1(\Phi), \ldots, v_N(\Phi)$ are given by

$$v_i(\Phi) := C(1 - \phi)V(\phi)(\delta_i - \boldsymbol{\delta}^{\mathrm{T}}\Phi), \quad \text{where} \quad \delta_i := D_i^2/D_1^2, \quad i = 1, \ldots, N,$$
$$\boldsymbol{\delta} := (\delta_1 = 1, \delta_2, \ldots, \delta_N)^{\mathrm{T}}, \quad C := \frac{\rho_s - \rho_f}{18\mu_f}gD_1^2, \tag{2.5}$$

where ρ_f is fluid density, g is the acceleration of gravity, μ_f is the fluid viscosity, $\phi := \phi_1 + \cdots + \phi_N$ is the total solids volume fraction, and $V(\phi)$ is a hindered settling factor that is assumed to satisfy $V(0) = 1$, $V(\phi_{\max}) = 0$, and $V'(\phi) \le 0$ for $\phi \in [0, \phi_{\max}]$. A standard choice is the Richardson-Zaki equation [48]

$$V(\phi) = \tilde{V}(\phi) := \begin{cases} (1 - \phi)^{n_{\mathrm{RZ}}-2} & \text{if } \Phi \in \mathcal{D}_{\phi_{\max}}, \\ 0 & \text{otherwise}, \end{cases} \quad n_{\mathrm{RZ}} > 3. \tag{2.6}$$

Following [18] and if $\phi_{\max} < 1$, we use a "soft cutoff" version of (2.6) to avoid the discontinuity at $\phi = \phi_{\max}$, namely

$$V(\phi) := \begin{cases} (1 - \phi)^{n_{\mathrm{RZ}}-2} & \text{for } 0 < \phi < \phi_*, \\ \tilde{V}(\phi_*) + \tilde{V}'(\phi_*)(\phi - \phi_*) & \text{for } \phi_* \le \phi \le \phi_{\max}, \quad n_{\mathrm{RZ}} > 3. \\ 0 & \text{otherwise}, \end{cases} \tag{2.7}$$

Here $\tau(\phi) := \tilde{V}(\phi_*) + \tilde{V}'(\phi_*)(\phi - \phi_*)$ is the tangent to $\tilde{V}(\phi)$ at $(\phi_*, \tilde{V}(\phi_*))$, where ϕ_* is chosen such that $\tau(\phi_{\max}) = 0$, i.e.,

$$\phi_* = \frac{(n_{\mathrm{RZ}} - 2)\phi_{\max} - 1}{n_{\mathrm{RZ}} - 3}.$$

According to [6], when $\phi_i > 0$ and $\phi < \phi_{\max}$, the MLB model is strictly hyperbolic and the eigenvalues $\lambda_i(\Phi)$ of the Jacobian matrix of the flux $\mathcal{J}_f(\Phi)$ interlace with the velocities $v_i(\Phi)$, as is expressed by (A.3) and where

$$M_1(\Phi) = C(\delta_N V(\phi) + ((1 - \phi)V'(\phi) - 2V(\phi))\boldsymbol{\delta}^{\mathrm{T}}\Phi), \quad M_2(\Phi) = v_1(\Phi). \tag{2.8}$$

5

In what follows we always assume that

$$V(\phi) > 0 \quad \text{for } 0 \le \phi < \phi_{\max}, \quad V(\phi_{\max}) = 0, \quad \text{and} \quad V'(\phi) \le 0. \tag{2.9}$$

These properties hold, for instance, if $V(\phi)$ is chosen according to (2.6), (2.7) with $0 < \phi_{\max} < 1$. The properties (2.9) ensure that (2.4) holds for the MLB model, where $M_1(\Phi)$ and $M_2(\Phi)$ are defined by (2.8). We may then choose $w(\phi) := C(1 - \phi)^2 V(\phi)$ and $\kappa := \delta$ along with $\psi(\phi) := C((1 - \phi)V'(\phi) - 2V(\phi))$ such that (1.5)–(1.9) are satisfied.

3. First-order invariant-region-preserving schemes

3.1. Discretizations

We first discretize the domain $[0, L] \times [0, T]$. For the spatial interval $[0, L]$, we choose $M \in \mathbb{N}$, a meshwidth $\Delta x := L/M$, and define the cell centers $x_j := (j + 1/2)\Delta x$ for $j \in \{0, \ldots, M - 1\}$ and the cell interfaces $x_{j+1/2} = (j + 1)\Delta x$ for $j \in \{0, \ldots, M\} =: \mathbb{Z}_M$. With this setup $x_{-1/2} = 0$ and $x_{M-1/2} = L$. In this way, we subdivide the interval $[0, L]$ into cells $I_j := [x_{j-1/2}, x_{j+1/2})$, $j \in \{0, \ldots, M - 1\}$. Similarly, for the time interval $[0, T]$ we select $N_T \in \mathbb{N}$ and a sequence of temporal mesh widths Δt_n, and defining $t_0 := 0$ and $t_{n+1} := t_n + \Delta t_n$ for $n \in \{0, \ldots, N_T\}$ subject to the condition $\Delta t_0 + \cdots + \Delta t_{N_T-1} = T$. This leads to time strips $I^n := [t_n, t_{n+1})$, $n \in \{0, \ldots, N_T - 1\}$. The ratio $\lambda_n := \Delta t_n / \Delta x$ is assumed to satisfy a CFL condition that will be specified later. The numerical schemes produce an approximation $\Phi_j^n \approx \Phi(x_j, t_n)$ defined at the mesh points (x_j, t_n) for $j \in \mathbb{Z}_M$ and $n \in \{0, \ldots, N_T\}$.

We then define a marching formula for the solution as

$$\Phi_j^{n+1} = \Phi_j^n - \lambda_n(\mathcal{F}_{j+1/2}^n - \mathcal{F}_{j-1/2}^n), \quad j = 0, \ldots, M - 1, \quad n = 0, \ldots, N_T - 1. \tag{3.1}$$

For the periodic boundary conditions (1.3), we set

$$\mathcal{F}_{-1/2}^n = \mathcal{F}_{M-1/2}^n, \tag{3.2}$$

and for the zero-flux boundary conditions (1.4),

$$\mathcal{F}_{-1/2}^n = \mathbf{0}, \quad \mathcal{F}_{M-1/2}^n = \mathbf{0}. \tag{3.3}$$

The computation of the numerical flux vector $\mathcal{F}_{j+1/2}^n$ in all other cases is described in what follows.

3.2. IRP property of the LLF scheme

We now describe a first-order method that satisfies the IRP property with respect to $\mathcal{D}_{\phi_{\max}}$. We utilize the local Lax-Friedrichs (LLF) numerical flux

$$\mathcal{F}_{j+1/2}^{\text{LLF}} := \frac{1}{2}(f(\Phi_j^n) + f(\Phi_{j+1}^n) - \alpha_{j+1/2}^n(\Phi_{j+1}^n - \Phi_j^n)), \quad \text{where} \quad \alpha_{j+1/2}^n := \max\{|S_{\text{L},j+1/2}^n|, |S_{\text{R},j+1/2}^n|\}, \tag{3.4}$$

where $S_{\text{L},j+1/2}^n$ and $S_{\text{R},j+1/2}^n$ denote lower and upper bounds for the eigenvalues $\lambda_1(\Phi), \ldots, \lambda_N(\Phi)$ of $\mathcal{J}_f(\Phi)$ at the interface $x_{j+1/2}$. These values can be estimated by setting

$$S_{\text{L},j+1/2}^n = \min_{0 \le s \le 1} M_1(s\Phi_{j+1}^n + (1 - s)\Phi_j^n), \tag{3.5}$$

$$S_{\text{R},j+1/2}^n = \max_{0 \le s \le 1} M_2(s\Phi_{j+1}^n + (1 - s)\Phi_j^n), \tag{3.6}$$

where M_1 and M_2 are given by (2.2) or (2.8) (depending on the model under study).

Now we can prove an IRP property for the first-order scheme (3.1), equipped with the LLF numerical flux (3.4). For the proof, we use a slightly smaller bound for the smallest eigenvalue than the one stipulated by (2.2) for the MCLWR model and by (2.8) for the MLB model; namely, we employ $\tilde{M}_1(\Phi) := \psi(\phi)\kappa^{\mathsf{T}}\Phi$, where we recall from Sections 2.1 and 2.2 that

$$\psi(\phi) := \begin{cases} v'(\phi) & \text{for the MCLWR model,} \\ C[(1 - \phi)V'(\phi) - 2V(\phi)] & \text{for the MLB model,} \end{cases} \qquad \kappa := \begin{cases} \beta & \text{for the MCLWR model,} \\ \delta & \text{for the MLB model.} \end{cases} \tag{3.7}$$

6

Notice that $\psi(\phi) \leq 0$ for $0 \leq \phi \leq \phi_{\max}$ for both models due to the explicit respective assumptions (2.3) and (2.9). For both models, $\tilde{M}_1(\Phi) \leq M_1(\Phi)$, and to prove the IRP property for both models and the LLF and HHL schemes we employ the slightly smaller lower estimate (instead of (3.5))

$$S^n_{\mathrm{L},j+1/2} = \min_{0 \leq s \leq 1} \tilde{M}_1(\Phi^n_{j+1/2}(s)), \quad \text{where} \quad \Phi^n_{j+1/2}(s) := s\Phi^n_{j+1} + (1-s)\Phi^n_j. \tag{3.8}$$

Theorem 1. *Consider the LLF scheme defined by the marching formula*

$$\Phi^{n+1}_j = \Phi^n_j - \lambda_n(\mathcal{F}^{\mathrm{LLF}}_{j+1/2} - \mathcal{F}^{\mathrm{LLF}}_{j-1/2}), \tag{3.9}$$

where the LLF numerical flux is given by (3.4) along with the definitions (3.6) and (3.8) of $S_{\mathrm{R},j+1/2}$ and $S_{\mathrm{L},j+1/2}$, respectively. If the CFL condition

$$\alpha\lambda_n \leq 1, \quad \text{where} \quad \alpha := \max_j\{|S_{\mathrm{L},j+1/2}|, |S_{\mathrm{R},j+1/2}|\} \tag{3.10}$$

is in effect, then the LLF scheme for (1.1), with the velocity functions $v_i(\Phi)$ chosen such that there exists a function $w = w(\phi)$ satisfying (1.5)–(1.9), satisfies the invariant region preservation property

$$\text{for all } n = 0, \ldots, N_T - 1: \quad \Phi^n_j \in \mathcal{D}_{\phi_{\max}} \quad \text{for all } j \in \mathbb{Z}_M \Rightarrow \Phi^{n+1}_j \in \mathcal{D}_{\phi_{\max}} \quad \text{for all } j \in \mathbb{Z}_M. \tag{3.11}$$

Proof. For simplicity, in the proof we omit the index n in the right-hand side of the marching formula, i.e., we set $\Phi_j := \Phi^n_j$, $\alpha_{j+1/2} := \alpha^n_{j+1/2}$, and $\lambda := \lambda_n$. Let us assume that both $\mathcal{F}^{\mathrm{LLF}}_{j+1/2}$ and $\mathcal{F}^{\mathrm{LLF}}_{j-1/2}$ are given by appropriate versions of (3.4) (see Remark 1 below for the boundary flux vectors defined by (3.2) or (3.3)). Then

$$\mathcal{F}^{\mathrm{LLF}}_{j+1/2} - \mathcal{F}^{\mathrm{LLF}}_{j-1/2} = \frac{\alpha_{j+1/2} + \alpha_{j-1/2}}{2}\Phi_j - \frac{\alpha_{j+1/2}}{2}\left(\Phi_{j+1} - \frac{1}{\alpha_{j+1/2}}f(\Phi_{j+1})\right) - \frac{\alpha_{j-1/2}}{2}\left(\Phi_{j-1} + \frac{1}{\alpha_{j-1/2}}f(\Phi_{j-1})\right),$$

hence by the marching formula (3.1) and defining

$$\mathcal{G}_1(\Phi_{j+1}) := \Phi_{j+1} - \frac{1}{\alpha_{j+1/2}}f(\Phi_{j+1}) \quad \text{and} \quad \mathcal{G}_2(\Phi_{j-1}) := \Phi_{j-1} + \frac{1}{\alpha_{j-1/2}}f(\Phi_{j-1}),$$

we can write

$$\Phi^{n+1}_j = \left(1 - \frac{\lambda(\alpha_{j+1/2} + \alpha_{j-1/2})}{2}\right)\Phi_j + \frac{\lambda\alpha_{j+1/2}}{2}\mathcal{G}_1(\Phi_{j+1}) + \frac{\lambda\alpha_{j-1/2}}{2}\mathcal{G}_2(\Phi_{j-1}). \tag{3.12}$$

Consequently, the CFL condition (3.10) implies that Φ^{n+1}_j can be represented as a convex combination of Φ_j, $\mathcal{G}_1(\Phi_{j+1})$, and $\mathcal{G}_2(\Phi_{j-1})$. Noting that

$$\mathcal{G}_{1,i}(\Phi_{j+1}) = \phi_{i,j+1} - \frac{f_i(\Phi_{j+1})}{\alpha_{j+1/2}} = \phi_{i,j+1}\left(1 - \frac{v_i(\Phi_{j+1})}{\alpha_{j+1/2}}\right) \geq \phi_{i,j+1}\left(1 - \frac{|v_1(\Phi_{j+1})|}{\alpha_{j+1/2}}\right) \geq \phi_{i,j+1}\left(1 - \frac{|S_{\mathrm{R},j+1/2}|}{\alpha_{j+1/2}}\right) \quad \text{and}$$

$$\mathcal{G}_{2,i}(\Phi_{j-1}) = \phi_{i,j-1} + \frac{f_i(\Phi_{j-1})}{\alpha_{j-1/2}} = \phi_{i,j-1}\left(1 + \frac{v_i(\Phi_{j-1})}{\alpha_{j-1/2}}\right) \geq \phi_{i,j-1}\left(1 + \frac{M_1(\Phi_{j-1})}{\alpha_{j-1/2}}\right) \geq \phi_{i,j-1}\left(1 + \frac{S_{\mathrm{L},j-1/2}}{\alpha_{j-1/2}}\right)$$

$$\geq \phi_{i,j-1}\left(1 - \frac{|S_{\mathrm{L},j-1/2}|}{\alpha_{j-1/2}}\right)$$

and recalling the definition of $\alpha_{j+1/2}$ in (3.4), we see that $\mathcal{G}_{1,i}(\Phi_{j+1}) \geq 0$ and $\mathcal{G}_{2,i}(\Phi_{j-1}) \geq 0$. Since the coefficients of $\phi_{i,j}$, $\phi_{i,j+1}$, and $\phi_{i,j-1}$ are all nonnegative (this follows in case of the coefficient of $\phi_{i,j}$ from the CFL condition), we deduce that if $\phi_{i,j} \geq 0$, $\phi_{i,j+1} \geq 0$, and $\phi_{i,j-1} \geq 0$, then $\phi^{n+1}_{i,j} \geq 0$ for all $i \in \{1, \ldots, N\}$.

It remains to prove that if $\phi_j := \phi^n_j := \phi^n_{1,j} + \cdots + \phi^n_{N,j} \leq \phi_{\max}$ for all j, then $\phi^{n+1}_j \leq \phi_{\max}$ for all j. Component i, $i \in \{1, \ldots, N\}$ of (3.12) can be rewritten as

$$\phi^{n+1}_{i,j} = \left(1 - \lambda\frac{\alpha_{j+1/2} + \alpha_{j-1/2}}{2}\right)\phi_{i,j} + \frac{\lambda\alpha_{j+1/2}}{2}\left(\phi_{i,j+1} - \frac{\phi_{i,j+1}v_i(\Phi_{j+1})}{\alpha_{j+1/2}}\right) + \frac{\lambda\alpha_{j-1/2}}{2}\left(\phi_{i,j-1} + \frac{\phi_{i,j-1}v_i(\Phi_{j-1})}{\alpha_{j-1/2}}\right)$$

$$= \left(1 - \lambda\frac{\alpha_{j+1/2} + \alpha_{j-1/2}}{2}\right)\phi_{i,j} + \frac{\lambda\alpha_{j+1/2}}{2}\phi_{i,j+1} + \frac{\lambda\alpha_{j-1/2}}{2}\phi_{i,j-1} - \frac{\lambda}{2}\phi_{i,j+1}v_i(\Phi_{j+1}) + \frac{\lambda}{2}\phi_{i,j-1}v_i(\Phi_{j-1}) \tag{3.13}$$

7

Summing (3.13) over $i = 1, \ldots, N$, we get

$$\phi_j^{n+1} = \left(1 - \lambda \frac{\alpha_{j+1/2} + \alpha_{j-1/2}}{2}\right)\phi_j + \frac{\lambda\alpha_{j+1/2}}{2}\phi_{i,j+1} + \frac{\lambda\alpha_{j-1/2}}{2}\phi_{i,j-1} - \frac{\lambda}{2}\sum_{i=1}^{N} v_i(\Phi_{j+1})\phi_{j+1} + \frac{\lambda}{2}\sum_{i=1}^{N} v_i(\Phi_{j-1})\phi_{j-1}. \quad (3.14)$$

According to (1.5), we can write (3.14) as

$$\phi_j^{n+1} = \left(1 - \lambda \frac{\alpha_{j+1/2} + \alpha_{j-1/2}}{2}\right)\phi_j + \frac{\lambda\alpha_{j+1/2}}{2}\phi_{j+1} + \frac{\lambda\alpha_{j-1/2}}{2}\phi_{j-1} - \frac{\lambda}{2}w(\phi_{j+1})\boldsymbol{\kappa}^{\mathrm{T}}\Phi_{j+1} + \frac{\lambda}{2}w(\phi_{j-1})\boldsymbol{\kappa}^{\mathrm{T}}\Phi_{j-1}. \quad (3.15)$$

In light of (1.6) we obtain

$$\phi_j^{n+1} \leq \left(1 - \lambda \frac{\alpha_{j+1/2} + \alpha_{j-1/2}}{2}\right)\phi_j + \frac{\lambda\alpha_{j+1/2}}{2}\phi_{j+1} + \frac{\lambda\alpha_{j-1/2}}{2}\phi_{j-1} + \frac{\lambda}{2}w(\phi_{j-1})\boldsymbol{\kappa}^{\mathrm{T}}\Phi_{j-1}$$

$$= \left(1 - \lambda \frac{\alpha_{j+1/2} + \alpha_{j-1/2}}{2}\right)\phi_j + \frac{\lambda\alpha_{j+1/2}}{2}\phi_{j+1} + \frac{\lambda\alpha_{j-1/2}}{2}\phi_{\max} + \mathcal{Y}, \quad (3.16)$$

where we define

$$\mathcal{Y} := \frac{\lambda}{2}\left(\alpha_{j-1/2}(\phi_{j-1} - \phi_{\max}) + w(\phi_{j-1})\boldsymbol{\kappa}^{\mathrm{T}}\Phi_{j-1}\right). \quad (3.17)$$

We assume that $\phi_j, \phi_{j+1} \in [0, \phi_{\max}]$. If $\phi_{j-1} = \phi_{\max}$ then $\mathcal{Y} = 0$, so we deduce from (1.7), by a convex combination argument, that $\phi_j^{n+1} \leq \phi_{\max}$. To handle the remaining cases, i.e. $0 \leq \phi_{j-1} < \phi_{\max}$, we divide (3.17) by $\phi_{j-1} - \phi_{\max}$ to obtain

$$\frac{\mathcal{Y}}{\phi_{j-1} - \phi_{\max}} = \frac{\lambda\alpha_{j-1/2}}{2} + \frac{\lambda}{2}\frac{w(\phi_{j-1})}{\phi_{j-1} - \phi_{\max}}\boldsymbol{\kappa}^{\mathrm{T}}\Phi_{j-1}. \quad (3.18)$$

Notice that there exists a number $\xi_{j-1} \in [\phi_{j-1}, \phi_{\max}]$ such that

$$\frac{w(\phi_{j-1})}{\phi_{j-1} - \phi_{\max}} = \frac{w(\phi_{j-1}) - w(\phi_{\max})}{\phi_{j-1} - \phi_{\max}} = w'(\xi_{j-1}) \geq w'(\phi_{j-1}),$$

where the last inequality holds due to (1.8). Consequently, from (3.18) and $\alpha_{j-1/2} \geq |S_{\mathrm{L},j-1/2}| \geq -S_{\mathrm{L},j-1/2}^-$ we get

$$\frac{\mathcal{Y}}{\phi_{j-1} - \phi_{\max}} \geq \frac{\lambda}{2}\left(-S_{\mathrm{L},j-1/2}^- + w'(\phi_{j-1})\boldsymbol{\kappa}^{\mathrm{T}}\Phi_{j-1}\right). \quad (3.19)$$

Since

$$S_{\mathrm{L},j-1/2}^- \leq S_{\mathrm{L},j-1/2} = \min_{0 \leq s \leq 1} \psi(\phi_{j-1/2}(s))\boldsymbol{\kappa}^{\mathrm{T}}\Phi_{j-1/2}(s) \leq \psi(\phi_{j-1})\boldsymbol{\kappa}^{\mathrm{T}}\Phi_{j-1} \leq w'(\phi_{j-1})\boldsymbol{\kappa}^{\mathrm{T}}\Phi_{j-1}, \quad (3.20)$$

we get that $-S_{\mathrm{L},j-1/2}^- \geq -w'(\phi_{j-1})\boldsymbol{\kappa}^{\mathrm{T}}\Phi_{j-1}$. Thus, after multiplying (3.19) with $\phi_{j-1} - \phi_{\max} < 0$, we get $\mathcal{Y} \leq 0$ and therefore, from (3.16),

$$\phi_j^{n+1} \leq \left(1 - \lambda \frac{\alpha_{j+1/2} + \alpha_{j-1/2}}{2}\right)\phi_j + \frac{\lambda\alpha_{j+1/2}}{2}\phi_{j+1} + \frac{\lambda\alpha_{j-1/2}}{2}\phi_{\max}.$$

The right-hand side is a convex combination of ϕ_j, ϕ_{j+1}, and $\phi_{\max}$, so if $\phi_j \in [0, \phi_{\max}]$ and $\phi_{j+1} \in [0, \phi_{\max}]$, then $\phi_j^{n+1} \leq \phi_{\max}$. This concludes the proof of Theorem 1. $\qquad\square$

Remark 1. *Clearly, the previous proof also handles the case of periodic boundary conditions (3.2) if we assume that the marching formula (3.9) verbatim for all $j = 0, \ldots, M-1$ but understand all indices j "modulo M", with the effect that (3.2) is indeed enforced. As for the zero-flux boundary conditions (3.3), consider for example the case $\mathcal{F}_{-1/2}^n = \mathbf{0}$. The corresponding boundary scheme then becomes*

$$\Phi_0^{n+1} = \Phi_0^n - \lambda\mathcal{F}_{1/2}^{\mathrm{LLF}} = \Phi_0^n - \frac{\lambda}{2}\left(f(\Phi_0^n) + f(\Phi_1^n) - \alpha_{1/2}^n(\Phi_1^n - \Phi_0^n)\right). \quad (3.21)$$

Simpler versions of the arguments used in the proof of Theorem 1 now suffice to show that also the boundary scheme (3.21) satisfies the IRP property. For instance, one may formally set $\mathcal{G}_2(\Phi_{-1}) := \mathbf{0}$ and $\alpha_{-1/2} := 0$ to demonstrate that $\phi_{i,0}^{n+1} \geq 0$ for all $i = 1, \ldots, N$, and $\phi_{-1} := \phi_{\max}$ and $\alpha_{-1/2} = 0$ in (3.16) to deduce that $\phi_0^{n+1} \leq \phi_{\max}$ (under the conditions stated in Theorem 1). The boundary condition $\mathcal{F}_{M-1/2}^n = \mathbf{0}$ is treated by similar arguments.

3.3. IRP property of the HLL scheme

Let us now consider the HLL scheme [27] defined by the numerical flux

$$\mathcal{F}_{j+1/2}^{\mathrm{HLL}} := \frac{S_{\mathrm{R},j+1/2}^{+} f(\Phi_j) - S_{\mathrm{L},j+1/2}^{-} f(\Phi_{j+1}) + S_{\mathrm{L},j+1/2}^{-} S_{\mathrm{R},j+1/2}^{+} (\Phi_{j+1} - \Phi_j)}{S_{\mathrm{R},j+1/2}^{+} - S_{\mathrm{L},j+1/2}^{-}}, \tag{3.22}$$

where $S_{\mathrm{L},j+1/2}$ and $S_{\mathrm{R},j+1/2}$ are defined as in (3.6), and we have used the notation $a^- = \min(a,0)$ and $a^+ = \max(a,0)$. First of all, observe that the HLL numerical flux (3.22) is well defined for both the MCLWR and MLB models, since (2.4) ensures that always

$$S_{\mathrm{L},j+1/2}^{-} < S_{\mathrm{R},j+1/2}^{+} \quad \text{for all } j. \tag{3.23}$$

For the proof of the invariant region principle of the HLL scheme, we also use the bound for the smallest eigenvalue stipulated by (3.7) and (3.8).

Theorem 2. *Consider the HLL scheme defined by the marching formula*

$$\Phi_j^{n+1} = \Phi_j^n - \lambda_n (\mathcal{F}_{j+1/2}^{\mathrm{HLL}} - \mathcal{F}_{j-1/2}^{\mathrm{HLL}}), \tag{3.24}$$

where the HLL numerical flux is given by (3.22) along with the definitions (3.6) and (3.8) of $S_{\mathrm{R},j+1/2}$ and $S_{\mathrm{L},j+1/2}$, respectively. If the CFL condition

$$\alpha \lambda_n \leq \frac{1}{2}, \quad \text{where} \quad \alpha := \max_{j} \{ |S_{\mathrm{L},j+1/2}|, |S_{\mathrm{R},j+1/2}| \} \tag{3.25}$$

is in effect, then the HLL scheme satisfies the invariant region preservation property (3.11) for the multispecies kinematic flow model (1.1) with the velocity functions $v_i(\Phi)$ chosen such that there exists a function $w = w(\phi)$ satisfying (1.5)–(1.9).

Proof. For simplicity, let us keep the same notation as in the proof of Theorem 1, i.e., we set $\Phi_j := \Phi_j^n$ and $\lambda := \lambda_n$. A straightforward computation reveals that the marching formula of the HLL scheme (3.24) can be written as follows, where we assume that $S_{\mathrm{R},j+1/2}^{+} > 0$, $S_{\mathrm{L},j+1/2}^{-} < 0$, $S_{\mathrm{R},j-1/2}^{+} > 0$, and $S_{\mathrm{L},j-1/2}^{-} < 0$:

$$
\begin{aligned}
\Phi_j^{n+1} = \Phi_j - \lambda \Bigg(& \frac{S_{\mathrm{R},j+1/2}^{+} f(\Phi_j) - S_{\mathrm{L},j+1/2}^{-} f(\Phi_{j+1}) + S_{\mathrm{L},j+1/2}^{-} S_{\mathrm{R},j+1/2}^{+} (\Phi_{j+1} - \Phi_j)}{S_{\mathrm{R},j+1/2}^{+} - S_{\mathrm{L},j+1/2}^{-}} \\
& - \frac{S_{\mathrm{R},j-1/2}^{+} f(\Phi_{j-1}) - S_{\mathrm{L},j-1/2}^{-} f(\Phi_j) + S_{\mathrm{L},j-1/2}^{-} S_{\mathrm{R},j-1/2}^{+} (\Phi_j - \Phi_{j-1})}{S_{\mathrm{R},j-1/2}^{+} - S_{\mathrm{L},j-1/2}^{-}} \Bigg) \\
= \Bigg(1 & + \frac{2\lambda S_{\mathrm{L},j+1/2}^{-} S_{\mathrm{R},j+1/2}^{+}}{S_{\mathrm{R},j+1/2}^{+} - S_{\mathrm{L},j+1/2}^{-}} + \frac{2\lambda S_{\mathrm{L},j-1/2}^{-} S_{\mathrm{R},j-1/2}^{+}}{S_{\mathrm{R},j-1/2}^{+} - S_{\mathrm{L},j-1/2}^{-}} \Bigg) \Phi_j + \frac{-\lambda S_{\mathrm{L},j+1/2}^{-} S_{\mathrm{R},j+1/2}^{+}}{S_{\mathrm{R},j+1/2}^{+} - S_{\mathrm{L},j+1/2}^{-}} \Bigg(\Phi_{j+1} - \frac{1}{S_{\mathrm{R},j+1/2}^{+}} f(\Phi_{j+1}) \Bigg) \\
& + \frac{-\lambda S_{\mathrm{L},j+1/2}^{-} S_{\mathrm{R},j+1/2}^{+}}{S_{\mathrm{R},j+1/2}^{+} - S_{\mathrm{L},j+1/2}^{-}} \Bigg(\Phi_j + \frac{1}{(-S_{\mathrm{L},j+1/2}^{-})} f(\Phi_j) \Bigg) + \frac{-\lambda S_{\mathrm{L},j-1/2}^{-} S_{\mathrm{R},j-1/2}^{+}}{S_{\mathrm{R},j-1/2}^{+} - S_{\mathrm{L},j-1/2}^{-}} \Bigg(\Phi_{j-1} + \frac{1}{(-S_{\mathrm{L},j-1/2}^{-})} f(\Phi_{j-1}) \Bigg) \\
& + \frac{-\lambda S_{\mathrm{L},j-1/2}^{-} S_{\mathrm{R},j-1/2}^{+}}{S_{\mathrm{R},j-1/2}^{+} - S_{\mathrm{L},j-1/2}^{-}} \Bigg(\Phi_j - \frac{1}{S_{\mathrm{R},j-1/2}^{+}} f(\Phi_j) \Bigg).
\end{aligned}
$$

Consequently, if we define the coefficients

$$\gamma_{j+1/2} := \frac{-S_{\mathrm{L},j+1/2}^{-} S_{\mathrm{R},j+1/2}^{+}}{S_{\mathrm{R},j+1/2}^{+} - S_{\mathrm{L},j+1/2}^{-}} > 0 \quad \text{for all } j \tag{3.26}$$

and the functions

$$\mathcal{G}_1(\Phi_{j+1}) := \Phi_{j+1} - \frac{1}{S_{\mathrm{R},j+1/2}^{+}} f(\Phi_{j+1}), \qquad \mathcal{G}_2(\Phi_j) := \Phi_j + \frac{1}{(-S_{\mathrm{L},j+1/2}^{-})} f(\Phi_j),$$

$$\mathcal{G}_3(\Phi_{j-1}) := \Phi_{j-1} + \frac{1}{(-S_{\mathrm{L},j-1/2}^{-})} f(\Phi_{j-1}), \qquad \mathcal{G}_4(\Phi_j) := \Phi_{j-1} - \frac{1}{S_{\mathrm{R},j-1/2}^{+}} f(\Phi_j),$$

9

then we obtain

$$\phi_{i,j}^{n+1} = (1 - 2(\gamma_{j+1/2} + \gamma_{j-1/2}))\phi_{i,j} + \gamma_{j+1/2}\mathcal{G}_{1,i}(\Phi_{j+1}) + \gamma_{j+1/2}\mathcal{G}_{2,i}(\Phi_j) + \gamma_{j-1/2}\mathcal{G}_{3,i}(\Phi_{j-1}) + \gamma_{j-1/2}\mathcal{G}_{4,i}(\Phi_j). \quad (3.27)$$

Since $\gamma_{j+1/2} > 0$ and $\gamma_{j-1/2} > 0$, under the CFL condition (3.25) this identity represents a convex combination of $\phi_{i,j}$, $\mathcal{G}_{1,i}(\Phi_{j+1})$, $\mathcal{G}_{2,i}(\Phi_j)$, $\mathcal{G}_{3,i}(\Phi_{j-1})$, and $\mathcal{G}_{4,i}(\Phi_j)$. If we assume that $\phi_{i,j} \geq 0$ for all $i = 1, \ldots, N$ and $j \in \mathbb{Z}_M$ and take into account that $f_i(\Phi) = \phi_i v_i(\Phi)$, then we get

$$\mathcal{G}_{1,i}(\Phi_{j+1}) = \phi_{i,j+1}\left(1 - \frac{v_i(\Phi_{j+1})}{S_{R,j+1/2}^+}\right) \geq \phi_{i,j+1}\left(1 - \frac{M_2(\Phi_{j+1})}{S_{R,j+1/2}^+}\right) \geq 0,$$

$$\mathcal{G}_{2,i}(\Phi_j) = \phi_{i,j}\left(1 + \frac{v_i(\Phi_j)}{(-S_{L,j+1/2}^-)}\right) \geq \phi_{i,j}\left(1 + \frac{M_1(\Phi_j)}{(-S_{L,j+1/2}^-)}\right) \geq 0,$$

$$\mathcal{G}_{3,i}(\Phi_{j-1}) = \phi_{i,j-1}\left(1 + \frac{v_i(\Phi_{j-1})}{(-S_{L,j-1/2}^-)}\right) \geq \phi_{i,j}\left(1 + \frac{M_1(\Phi_{j-1})}{(-S_{L,j-1/2}^-)}\right) \geq 0,$$

$$\mathcal{G}_{4,i}(\Phi_j) = \phi_{i,j}\left(1 - \frac{v_i(\Phi_j)}{S_{R,j-1/2}^+}\right) \geq \phi_{i,j}\left(1 - \frac{M_2(\Phi_j)}{S_{R,j-1/2}^+}\right) \geq 0.$$

Thus, $\mathcal{G}_{k,i}(\Phi_j) \geq 0$ for all $i = 1, \ldots, N$, $k = 1, \ldots, 4$, and $j \in \mathbb{Z}_M$. Since the coefficient of $\phi_{i,j}$ is non-negative (this follows from the CFL condition), we deduce that if $\phi_{i,j} \geq 0$, $\phi_{i,j+1} \geq 0$, and $\phi_{i,j-1} \geq 0$, then $\phi_{i,j}^{n+1} \geq 0$.

It remains to prove that if $\phi_j \leq \phi_{\max}$ for all j, then $\phi_j^{n+1} \leq \phi_{\max}$ for all j. To this end, we rewrite (3.27) as

$$\phi_{i,j}^{n+1} = \left(1 - \lambda\frac{S_{R,j+1/2}^+}{S_{R,j+1/2}^+ - S_{L,j+1/2}^-}(v_i(\Phi_j) - S_{L,j+1/2}^-) + \frac{\lambda S_{L,j-1/2}^-}{S_{R,j-1/2}^+ - S_{L,j-1/2}^-}(S_{R,j-1/2}^+ - v_i(\Phi_j))\right)\phi_{i,j}$$

$$+ \frac{-\lambda S_{L,j+1/2}^-}{S_{R,j+1/2}^+ - S_{L,j+1/2}^-}(S_{R,j+1/2}^+ - v_i(\Phi_{j+1}))\phi_{i,j+1} + \frac{\lambda S_{R,j-1/2}^+}{S_{R,j-1/2}^+ - S_{L,j-1/2}^-}(v_i(\Phi_{j-1}) - S_{L,j-1/2}^-)\phi_{i,j-1}. \quad (3.28)$$

Summing (3.28) over $i = 1, \ldots, N$, we get

$$\phi_j^{n+1} = \sum_{i=1}^N\left(1 - \lambda\frac{S_{R,j+1/2}^+}{S_{R,j+1/2}^+ - S_{L,j+1/2}^-}(v_i(\Phi_j) - S_{L,j+1/2}^-) + \frac{\lambda S_{L,j-1/2}^-}{S_{R,j-1/2}^+ - S_{L,j-1/2}^-}(S_{R,j-1/2}^+ - v_i(\Phi_j))\right)\phi_{i,j}$$

$$+ \sum_{i=1}^N\frac{-\lambda S_{L,j+1/2}^-}{S_{R,j+1/2}^+ - S_{L,j+1/2}^-}(S_{R,j+1/2}^+ - v_i(\Phi_{j+1}))\phi_{i,j+1} + \sum_{i=1}^N\frac{\lambda S_{R,j-1/2}^+}{S_{R,j-1/2}^+ - S_{L,j-1/2}^-}(v_i(\Phi_{j-1}) - S_{L,j-1/2}^-)\phi_{i,j-1}. \quad (3.29)$$

From (3.29), we get

$$\phi_j^{n+1} = (1 - \lambda\gamma_{j+1/2} - \lambda\gamma_{j-1/2})\phi_j + \lambda\gamma_{j+1/2}\phi_{j+1} + \lambda\gamma_{j-1/2}\phi_{j-1}$$

$$- \frac{\lambda S_{L,j-1/2}^-}{S_{R,j-1/2}^+ - S_{L,j-1/2}^-}\sum_{i=1}^N v_i(\Phi_j)\phi_{i,j} - \frac{\lambda S_{R,j+1/2}^+}{S_{R,j+1/2}^+ - S_{L,j+1/2}^-}\sum_{i=1}^N v_i(\Phi_j)\phi_{i,j}$$

$$+ \frac{\lambda S_{L,j+1/2}^-}{S_{R,j+1/2}^+ - S_{L,j+1/2}^-}\sum_{i=1}^N v_i(\Phi_{j+1})\phi_{i,j+1} + \frac{\lambda S_{R,j-1/2}^+}{S_{R,j-1/2}^+ - S_{L,j-1/2}^-}\sum_{i=1}^N v_i(\Phi_{j-1})\phi_{i,j-1}. \quad (3.30)$$

Utilizing (1.5) we may rewrite this identity as

$$\phi_j^{n+1} = (1 - \lambda\gamma_{j+1/2} - \lambda\gamma_{j-1/2})\phi_j + \lambda\gamma_{j+1/2}\phi_{j+1} + \lambda\gamma_{j-1/2}\phi_{j-1}$$

$$- \frac{\lambda S_{L,j-1/2}^- w(\phi_j)\boldsymbol{\kappa}^{\mathrm{T}}\Phi_j}{S_{R,j-1/2}^+ - S_{L,j-1/2}^-} - \frac{\lambda S_{R,j+1/2}^+ w(\phi_j)\boldsymbol{\kappa}^{\mathrm{T}}\Phi_j}{S_{R,j+1/2}^+ - S_{L,j+1/2}^-} + \frac{\lambda S_{L,j+1/2}^- w(\phi_{j+1})\boldsymbol{\kappa}^{\mathrm{T}}\Phi_{j+1}}{S_{R,j+1/2}^+ - S_{L,j+1/2}^-} + \frac{\lambda S_{R,j-1/2}^+ w(\phi_{j-1})\boldsymbol{\kappa}^{\mathrm{T}}\Phi_{j-1}}{S_{R,j-1/2}^+ - S_{L,j-1/2}^-}. \quad (3.31)$$

10

Since by (1.6), the second and third term in the second line of the right-hand side of (3.31) are nonpositive, we get

$$\phi_j^{n+1} \le (1 - \lambda\gamma_{j+1/2} - \lambda\gamma_{j-1/2})\phi_j + \lambda\gamma_{j+1/2}\phi_{j+1} + \lambda\gamma_{j-1/2}\phi_{j-1} - \frac{\lambda S_{\text{L},j-1/2}^- w(\phi_j)\boldsymbol{\kappa}^\text{T}\Phi_j}{S_{\text{R},j-1/2}^+ - S_{\text{L},j-1/2}^-} + \frac{\lambda S_{\text{R},j-1/2}^+ w(\phi_{j-1})\boldsymbol{\kappa}^\text{T}\Phi_{j-1}}{S_{\text{R},j-1/2}^+ - S_{\text{L},j-1/2}^-}.$$
(3.32)

If we assume that $\phi_j = \phi_{\max}$, $\phi_{j-1} = \phi_{\max}$, and $\phi_{j+1} \in [0, \phi_{\max}]$, then we deduce from (1.7), by a convex combination argument, that $\phi_j^{n+1} \le \phi_{\max}$. To handle the remaining cases, we rewrite (3.32) as

$$\phi_j^{n+1} \le \left(\frac{1}{2} - \lambda\gamma_{j+1/2}\right)\phi_j + \left(\frac{1}{2} - \lambda\gamma_{j-1/2}\right)\phi_{\max} + \lambda\gamma_{j+1/2}\phi_{j+1} + \lambda\gamma_{j-1/2}\phi_{\max} + \mathcal{Y}_1 + \mathcal{Y}_2,$$

where we define

$$\mathcal{Y}_1 := \lambda\gamma_{j-1/2}(\phi_{j-1} - \phi_{\max}) + \frac{\lambda S_{\text{R},j-1/2}^+ w(\phi_{j-1})\boldsymbol{\kappa}^\text{T}\Phi_{j-1}}{S_{\text{R},j-1/2}^+ - S_{\text{L},j-1/2}^-},$$
(3.33)

$$\mathcal{Y}_2 := \left(\frac{1}{2} - \lambda\gamma_{j-1/2}\right)(\phi_j - \phi_{\max}) - \frac{\lambda S_{\text{L},j-1/2}^- w(\phi_j)\boldsymbol{\kappa}^\text{T}\Phi_j}{S_{\text{R},j-1/2}^+ - S_{\text{L},j-1/2}^-}.$$
(3.34)

If $\phi_{j-1} = \phi_{\max}$, then $\mathcal{Y}_1 = 0$; otherwise we may divide (3.33) by $\phi_{j-1} - \phi_{\max}$ to obtain

$$\frac{\mathcal{Y}_1}{\phi_{j-1} - \phi_{\max}} = \lambda\gamma_{j-1/2} + \lambda\frac{S_{\text{R},j-1/2}^+}{S_{\text{R},j-1/2}^+ - S_{\text{L},j-1/2}^-}\frac{w(\phi_{j-1})}{\phi_{j-1} - \phi_{\max}}\boldsymbol{\kappa}^\text{T}\Phi_{j-1}.$$
(3.35)

Notice that there exists a number $\xi_{j-1} \in [\phi_{j-1}, \phi_{\max}]$ such that

$$\frac{w(\phi_{j-1})}{\phi_{j-1} - \phi_{\max}} = \frac{w(\phi_{j-1}) - w(\phi_{\max})}{\phi_{j-1} - \phi_{\max}} = w'(\xi_{j-1}) \ge w'(\phi_{j-1}),$$

where we have used (1.8) to establish the last inequality. Thus, from (3.35) we get

$$\frac{\mathcal{Y}_1}{\phi_{j-1} - \phi_{\max}} \ge \lambda\frac{S_{\text{R},j-1/2}^+}{S_{\text{R},j-1/2}^+ - S_{\text{L},j-1/2}^-}(-S_{\text{L},j-1/2}^- + w'(\phi_{j-1})\boldsymbol{\kappa}^\text{T}\Phi_{j-1}).$$
(3.36)

Arguing exactly as in the discussion of inequality (3.19) in the proof of Theorem 1, we now deduce from (3.36) that $\mathcal{Y}_1/(\phi_{j-1} - \phi_{\max}) \ge 0$, and therefore $\mathcal{Y}_1 \le 0$. Furthermore, if $\phi_j = \phi_{\max}$, then $\mathcal{Y}_2 = 0$, otherwise we may divide (3.34) by $\phi_j - \phi_{\max}$ to obtain

$$\frac{\mathcal{Y}_2}{\phi_j - \phi_{\max}} = \frac{1}{2} - \lambda\gamma_{j-1/2} - \lambda\frac{S_{\text{L},j-1/2}^-}{S_{\text{R},j-1/2}^+ - S_{\text{L},j-1/2}^-}\frac{w(\phi_j)}{\phi_j - \phi_{\max}}\boldsymbol{\kappa}^\text{T}\Phi_j.$$

In light of (3.25), noticing that there exists $\xi_j \in [\phi_j, \phi_{\max}]$ such that

$$\frac{w(\phi_j)}{\phi_j - \phi_{\max}} = \frac{w(\phi_j) - w(\phi_{\max})}{\phi_j - \phi_{\max}} = w'(\xi_j) \ge w'(\phi_j)$$

(where we once again utilize (1.8)), taking into account that analogously to (3.20),

$$S_{\text{L},j-1/2}^- \le S_{\text{L},j-1/2} = \min_{0 \le s \le 1} \psi(\phi_{j-1/2}(s))\boldsymbol{\kappa}^\text{T}\Phi_{j-1/2}(s) \le \psi(\phi_j)\boldsymbol{\kappa}^\text{T}\Phi_j \le w'(\phi_j)\boldsymbol{\kappa}^\text{T}\Phi_j,$$
(3.37)

hence $-S_{\text{L},j-1/2}^- \ge -w'(\phi_j)\boldsymbol{\kappa}^\text{T}\Phi_j$, and appealing to the CFL condition, we obtain

$$\frac{\mathcal{Y}_2}{\phi_j - \phi_{\max}} = \frac{1}{2} - \lambda\frac{-S_{\text{L},j-1/2}^-}{S_{\text{R},j-1/2}^+ - S_{\text{L},j-1/2}^-}\left(S_{\text{R},j-1/2}^+ - w'(\xi_j)\boldsymbol{\kappa}^\text{T}\Phi_j\right) \ge \frac{1}{2} + \lambda S_{\text{L},j-1/2}^- \ge 0,$$

11

and therefore $\mathcal{Y}_2 \leq 0$. Consequently, we deduce that $\mathcal{Y}_1 + \mathcal{Y}_2 \leq 0$ which in the present case means that

$$\phi_j^{n+1} \leq \left(\frac{1}{2} - \lambda \gamma_{j+1/2}\right)\phi_j + \left(\frac{1}{2} - \lambda \gamma_{j-1/2}\right)\phi_{\max} + \lambda \gamma_{j+1/2}\phi_{j+1} + \lambda \gamma_{j-1/2}\phi_{\max}.$$

The right-hand side is a convex combination of ϕ_j, ϕ_{j+1}, and $\phi_{\max}$, so if $\phi_j \in [0, \phi_{\max}]$ and $\phi_{j+1} \in [0, \phi_{\max}]$, then $\phi_j^{n+1} \leq \phi_{\max}$. Thus, we always get $\phi_j^{n+1} \leq \phi_{\max}$. This concludes the proof of Theorem 2. $\qquad\square$

Remark 2. *A remark similar to Remark 1 is in place here. First of all, note that a simpler proof of $\phi_{i,j}^{n+1} \geq 0$ applies if one or two of the bounds $S_{\mathrm{R},j+1/2}^+$, $S_{\mathrm{L},j+1/2}^-$, $S_{\mathrm{R},j-1/2}^+$, and $S_{\mathrm{L},j-1/2}^-$ are zero (we recall that (3.23) is always in effect). In the latter case we have, of course, $\gamma_{j-1/2} = 0$ or $\gamma_{j+1/2} = 0$ (cf. (3.26)). On the other hand, as for the LLF scheme, it suffices to take all j-indices "modulo M" to demonstrate that the proof of of Theorem 2 also handles periodic boundary conditions. In the case of zero-flux boundary conditions (3.3), the bound $\phi_{i,j}^{n+1} \geq 0$ for $j = 0$ or $j = M - 1$ follows by taking into account that certain terms in the discussion leading to (3.27) are zero. With respect to the upper bound of ϕ_0^{n+1}, we note that if $\mathcal{F}_{-1/2}^n = \mathbf{0}$, then $\gamma_{-1/2} = 0$ and the last two terms on the right-hand side of (3.32) are zero, and we deduce that $\phi_0^{n+1} \leq \phi_{\max}$ by applying a standard convex combination argument to the remaining inequality. For $j = M - 1$, and considering the boundary condition $\mathcal{F}_{M-1/2}^n = \mathbf{0}$, (3.27) is valid for $j = M - 1$ if we set $\gamma_{M-1/2} = 0$. The remainder of the proof for both models remains valid. Consequently, Theorems 1 and 2 remain valid if appropriate numerical fluxes in the respective marching formulas (3.9) and (3.24) are replaced by boundary fluxes coming from (3.2) or (3.3).*

Remark 3. *Notice that the CFL conditions (3.10) and (3.25) are utilized to calculate Δt adaptively in every time step. However, one may employ a more restrictive but fixed CFL condition defined by bounds for $M_1(\Phi)$ and $M_2(\Phi)$. For instance, for the MCLWR model one may employ the condition $\lambda \max\{\beta_1\|v\|_\infty, \beta_1\phi_{\max}\|\psi\|_\infty\} \leq \mu$, while for MLB model one can consider $\lambda \max\{\delta_1\|w_1\|_\infty, \delta_1\phi_{\max}\|\psi\|_\infty\} \leq \mu$, where $w_1(\phi) = C(1-\phi)V(\phi)$, ψ is defined by (3.7), and*

$$\mu = \begin{cases} 1 & \text{for the LLF scheme,} \\ 1/2 & \text{for the HLL scheme.} \end{cases} \tag{3.38}$$

4. Invariant-region-preserving WENO reconstruction

4.1. Weighted essentially non-oscillatory (WENO) reconstruction (scalar case)

The WENO reconstruction [22] for the initial value problem of a one-dimensional scalar conservation law

$$\partial_t u + \partial_x f(u) = 0, \quad x \in \mathbb{R}, \quad t \in (0, T); \quad u(x, 0) = u_0(x), \quad x \in \mathbb{R}$$

is independent of the time variable, hence it is sufficient to consider $u = u(x)$ as a function of the spatial coordinate only. We define the cell averages $\bar{u}_j$ of u over all cells $I_j := [x_{j-1/2}, x_{j+1/2}]$:

$$\bar{u}_j := \frac{1}{\Delta x} \int_{x_{j-1/2}}^{x_{j+1/2}} u(x)\,\mathrm{d}x, \quad j \in \mathbb{Z}.$$

In what follows, Π_R denotes the set of all polynomials with real coefficients of maximal degree $R \in \mathbb{N}_0$.

Definition 1. *Consider a set of data (point values or cell averages) and a polynomial $P_{\mathrm{opt}} \in \Pi_R$, which interpolates in the appropriate sense all the given data (optimal polynomial). The WENO operator computes a reconstruction polynomial $P_{\mathrm{rec}} = \mathrm{WENO}(P_{\mathrm{opt}}, P_1, \ldots, P_m) \in \Pi_R$ from $P_{\mathrm{opt}} \in \Pi_R$ and a set of m lower-order alternative polynomials $P_1, \ldots, P_m \in \Pi_r$, where $r < R$ and $m \geq 1$. The definition of P_{rec} depends on the choice of a set of real coefficients*

$$C_0, C_1, \ldots, C_m \in [0, 1], \quad \text{where} \quad C_0 + C_1 + \cdots + C_m = 1, \quad C_0 > 0,$$

the so-called "linear weights," as follows:

   1. *First, we define $P_0 \in \Pi_R$ by*

$$P_0(x) := \frac{1}{C_0}\left(P_{\mathrm{opt}}(x) - \sum_{k=1}^{m} C_k P_k(x)\right).$$

2. *Then the nonlinear weights $\omega_0, \ldots, \omega_m$ are computed from the linear ones as*

$$\alpha_k := \frac{C_k}{(IS_k + \varepsilon)^p}, \quad \omega_k := \frac{\alpha_k}{\alpha_0 + \cdots + \alpha_m}, \quad k = 0, \ldots, m, \tag{4.1}$$

where $\varepsilon > 0$ is a small parameter, $p \geq 2$, and IS_k denotes a suitable regularity indicator, e.g. the Jiang-Shu indicator [23]

$$IS_k := \sum_{\ell=1}^{\text{degree}(P_k)} \Delta x^{2\ell-1} \int_{x_{j-1/2}}^{x_{j+1/2}} \left(\frac{\mathrm{d}^\ell P_k(x)}{\mathrm{d}x^\ell} \right)^2 \mathrm{d}x, \quad k = 0, \ldots, m.$$

3. *Finally, the reconstruction polynomial $P_{\text{rec}} \in \Pi_R$ is defined as*

$$P_{\text{rec}}(x) := \omega_0 P_0(x) + \omega_1 P_1(x) + \cdots + \omega_m P_m(x). \tag{4.2}$$

The reconstructed values of u at the boundaries $x_{i-1/2}$ and $x_{j+1/2}$ of cell I_j are now given by

$$u_{j-1/2}^{\text{R}} := P_{\text{rec}}(x_{j-1/2}), \quad u_{j+1/2}^{\text{L}} := P_{\text{rec}}(x_{j+1/2}). \tag{4.3}$$

Thus, based on cell averages $\bar{u}_j$ over all I_j, a WENO reconstruction of order $2r + 1$ ($r \in \{1, 2\}$ within this work), we consider on each interval a polynomial $P_{\text{opt}} \in \Pi_{R=2r}$ along with $m = r + 1$ polynomials $P_1, \ldots, P_{r+1} \in \Pi_r$ defined by

$$P_{\text{opt}}(x) := \sum_{s=0}^{2r} a_s^{(0)}(x - x_j)^s \quad \text{and} \quad P_k(x) := \sum_{s=0}^{r} a_s^{(k)}(x - x_j)^s, \quad k = 1, \ldots, r + 1,$$

where P_{opt} and P_k interpolate the cell averages associated with the respective stencils

$$S_0 = \bigcup_{\ell=-r}^{r} I_{j+\ell}, \quad \text{and} \quad S_k = \bigcup_{\ell=0}^{r} I_{j-r+k+\ell-1}, \quad k = 1, \ldots, r + 1.$$

For a fixed cell I_j these polynomials satisfy

$$\frac{1}{\Delta x} \int_{I_{j+\ell}} P_{\text{opt}}(x) \, \mathrm{d}x = \bar{u}_{j+\ell}, \quad \ell = -r, \ldots, r,$$

$$\frac{1}{\Delta x} \int_{I_{j-r+k+\ell-1}} P_k(x) \, \mathrm{d}x = \bar{u}_{j-r+k+\ell-1}, \quad \ell = 0, \ldots, r, \quad k = 1, \ldots, r + 1.$$

The reconstructed values (4.3) are easily computable since

$$P_0(x_{j\pm1/2}) = \sum_{s=0}^{2r} a_s^{(0)} \left(\pm \frac{\Delta x}{2} \right)^s = \sum_{s=0}^{2r} \alpha_s^{(0)} \bar{u}_{j+s-r} \quad \text{and}$$

$$P_k(x_{j\pm1/2}) = \sum_{\ell=0}^{r} a_\ell^{(k)} \left(\pm \frac{\Delta x}{2} \right)^\ell = \sum_{\ell=0}^{r} \alpha_\ell^{(k)} \bar{u}_{j-r+k+\ell-1}, \quad k = 1, \ldots, r + 1.$$

4.2. WENO reconstruction for systems of conservation laws

Let us consider a first-order IRP numerical flux $\mathcal{F}_{j+1/2}^n$ for (1.1), for instance the LLF flux (3.4) or the HLL flux (3.22). To describe WENO reconstructions for (1.1), we define $\mathcal{F}(\Phi_j^n, \Phi_{j+1}^n) := \mathcal{F}_{j+1/2}^n$, so we can write (3.1) as

$$\Phi_j^{n+1} = \Phi_j^n - \lambda_n \big(\mathcal{F}(\Phi_j^n, \Phi_{j+1}^n) - \mathcal{F}(\Phi_{j-1}^n, \Phi_j^n) \big). \tag{4.4}$$

In this work, we will use a component-wise WENO reconstruction, i.e.,

$$\Phi_{j+1/2}^{\text{L}} := (\phi_{1,j+1/2}^{\text{L}}, \ldots, \phi_{N,j+1/2}^{\text{L}})^{\text{T}}, \quad \Phi_{j+1/2}^{\text{R}} := (\phi_{1,j+1/2}^{\text{R}}, \ldots, \phi_{N,j+1/2}^{\text{R}})^{\text{T}},$$

$$\text{where} \quad \phi_{i,j-1/2}^{\text{R}} := P_j^{(i)}(x_{j-1/2}), \quad \phi_{i,j+1/2}^{\text{L}} := P_j^{(i)}(x_{j+1/2}), \quad i = 1, \ldots, N,$$

and $P_j^{(i)}$ denotes the reconstruction polynomial given by (4.2) for $i = 1, \ldots, N$. Then, we replace (4.4) by the WENO marching formula

$$\Phi_j^{n+1} = \Phi_j^n - \lambda_n(\mathcal{F}(\Phi_{j+1/2}^{\mathrm{L}}, \Phi_{j+1/2}^{\mathrm{R}}) - \mathcal{F}(\Phi_{j-1/2}^{\mathrm{L}}, \Phi_{j-1/2}^{\mathrm{R}})), \tag{4.5}$$

where

$$\Phi_{j-1/2}^{\mathrm{R}} := \boldsymbol{P}_j(x_{j-1/2}), \quad \Phi_{j+1/2}^{\mathrm{L}} := \boldsymbol{P}_j(x_{j+1/2}), \tag{4.6}$$

and we define the vector of polynomials $\boldsymbol{P}_j := (P_j^{(1)}, \ldots, P_j^{(N)})^{\mathrm{T}}$. In addition, to have the correct order of convergence of the method we need to use high-order time integration schemes; we focus on this aspect later.

4.3. Zhang and Shu limiters for multispecies kinematic flow models

It is well known that the reconstruction procedure described in Section 4 leads to schemes that resolve discontinuities sharply but in some cases fail to preserve the invariant region $\mathcal{D}_{\phi_{\max}}$ (see Examples 2 to 5 in Section 5 or numerical examples in [15, 16, 18]). This shortcoming motivated the development of the linear scaling limiter by Zhang and Shu [8]. We herein slightly modify this limiter to handle equations of the form (1.1).

The first step is to limit each concentration ϕ_i. Let us assume that $\Phi_j^n \in \mathcal{D}_{\phi_{\max}}^\delta$ for some small number $\delta > 0$, where

$$\mathcal{D}_{\phi_{\max}}^\delta := \{\Phi \in \mathbb{R}^N : \phi_1 \geq \delta, \ldots, \phi_N \geq \delta, \phi := \phi_1 + \cdots + \phi_N \leq \phi_{\max}\}.$$

For example, in all our numerical tests we set $\delta = 10^{-12}$. We then replace the polynomials $P_j^{(i)}(x)$ by

$$\tilde{P}_j^{(i)}(x) := \theta_i(P_j^{(i)}(x) - \phi_{i,j}^n) + \phi_{i,j}^n, \quad \theta_i := \min\left\{\frac{\phi_{i,j}^n - \delta}{\phi_{i,j}^n - m_j^{(i)}}, 1\right\}, \quad m_j^{(i)} := \min_{x \in I_j} P_j^{(i)}(x), \quad i = 1, \ldots, N. \tag{4.7}$$

Then the cell average of $\tilde{P}_j^{(i)}(x)$ over I_j is still $\phi_{i,j}^n$ and $\tilde{P}_j^{(i)}(x) \geq 0$ for all $x \in I_j$ and $i = 1, \ldots, N$. Next, we define the polynomial

$$\hat{P}_j(x) := \hat{\theta}\left(\sum_{i=1}^N \tilde{P}_j^{(i)}(x) - \phi_j^n\right) + \phi_j^n, \quad \hat{\theta} := \min\left\{\left|\frac{\phi_{\max} - \phi_j^n}{M_j - \phi_j^n}\right|, 1\right\}, \quad M_j := \max_{x \in I_j}\left(\sum_{i=1}^N \tilde{P}_j^{(i)}(x)\right). \tag{4.8}$$

Thus, $\hat{P}_j(x) \leq \phi_{\max}$ for all $x \in I_j$. Finally, we define the modified polynomials

$$\bar{P}_j^{(i)}(x) := \hat{\theta}(\tilde{P}_j^{(i)}(x) - \phi_{i,j}^n) + \phi_{i,j}^n, \quad i = 1, \ldots, N, \tag{4.9}$$

and replace the reconstructed values (4.6) by

$$\Phi_{j-1/2}^{\mathrm{R}} = \bar{\boldsymbol{P}}_j(x_{j-1/2}), \quad \Phi_{j+1/2}^{\mathrm{L}} = \bar{\boldsymbol{P}}_j(x_{j+1/2}). \tag{4.10}$$

The quantities $m_j^{(i)}$ in (4.7) and M_j in (4.8) require evaluating the extrema of polynomials on each cell. This inconvenience can be avoided if we define simplified limiters (as in [8]) that reduce the evaluations of each polynomial to a finite number of nodes of a G-point Legendre-Gauss-Lobatto quadrature rule on the interval $I_j = [x_{j-1/2}, x_{j+1/2}]$. This formula is exact for the integral of polynomials of degree up to $2G - 3$. We denote the quadrature points on I_j by

$$S_j := \{x_{j-1/2} = \hat{x}_j^1, \hat{x}_j^2, \ldots, \hat{x}_j^{G-1}, \hat{x}_j^G = x_{j+1/2}\}. \tag{4.11}$$

Let $\hat{w}_\alpha$ be the quadrature weights for the interval $[-1/2, 1/2]$ such that $\hat{w}_1 + \cdots + \hat{w}_G = 1$. For instance, we have used a three-point ($G = 3$) rule with weights

$$\hat{w}_1 = \frac{1}{6}, \quad \hat{w}_2 = \frac{2}{3}, \quad \hat{w}_3 = \frac{1}{6}$$

and a four-point ($G = 4$) rule with weights

$$\hat{w}_1 = \frac{1}{12}, \quad \hat{w}_2 = \frac{5}{12}, \quad \hat{w}_3 = \frac{5}{12}, \quad \hat{w}_4 = \frac{1}{12}$$

for the third and fifth order WENO reconstructions, respectively (notice that $\hat{w}_1 = \hat{w}_G$). Then we can write

$$\Phi_j^n = \frac{1}{\Delta x} \int_{I_j} \bar{\boldsymbol{P}}_j(x)\, \mathrm{d}x = \sum_{\alpha=1}^{G} \hat{w}_\alpha \bar{\boldsymbol{P}}_j(\hat{x}_j^\alpha) = \sum_{\alpha=2}^{G-1} \hat{w}_\alpha \bar{\boldsymbol{P}}_j(\hat{x}_j^\alpha) + \hat{w}_1 \Phi_{j-1/2}^R + \hat{w}_G \Phi_{j+1/2}^L. \tag{4.12}$$

We first prove the following lemma related to the polynomials $\bar{\boldsymbol{P}}_j := (\bar{P}_j^{(1)}, \ldots, \bar{P}_j^{(N)})^{\mathrm{T}}$.

Lemma 1. *Consider the reconstruction polynomials $\bar{\boldsymbol{P}}_j(x)$ defined by (4.9). If $\Phi_j^n \in \mathcal{D}_{\phi_{\max}}$, then $\bar{\boldsymbol{P}}_j(x) \in \mathcal{D}_{\phi_{\max}}$ for all $x \in I_j$. In particular, this is true for all $x \in S_j$, where S_j is the stencil (4.11) of Legendre-Gauss-Lobatto quadrature points for I_j.*

Proof. Let $x \in I_j$. By definition, we know that

$$\bar{P}_j^{(i)}(x) = \hat{\theta}(\tilde{P}_j^{(i)}(x) - \phi_{i,j}^n) + \phi_{i,j}^n = \hat{\theta}\tilde{P}_j^{(i)}(x) + (1 - \hat{\theta})\phi_{i,j}^n, \quad i = 1, \ldots, N. \tag{4.13}$$

Since $0 \le \hat{\theta} \le 1$ and $\tilde{P}_j^{(i)}(x) \ge 0$, there holds $\bar{P}_j^{(i)}(x) \ge 0$ for $i = 1, \ldots, N$. In addition, by (4.8),

$$\sum_{i=1}^{N} \bar{P}_j^{(i)}(x) = \hat{\theta}\left(\sum_{i=1}^{N} \tilde{P}_j^{(i)}(x) - \sum_{i=1}^{N} \phi_{i,j}^n\right) + \sum_{i=1}^{N} \phi_{i,j}^n = \hat{\theta}\left(\sum_{i=1}^{N} \tilde{P}_j^{(i)}(x) - \phi_j^n\right) + \phi_j^n = \hat{P}_j(x) \le \phi_{\max}. \tag{4.14}$$

Combining (4.13) and (4.14) we deduce that $\bar{\boldsymbol{P}}_j(x) \in \mathcal{D}_{\phi_{\max}}$ for all $x \in I_j$. $\qquad\square$

Now, we are in position to state the following result.

Theorem 3. *Consider the finite volume scheme (4.5) associated with the reconstruction polynomials $\bar{\boldsymbol{P}}_j(x)$ defined by (4.9) in the sense that (4.10) is used, and where the quantities $m_j^{(i)}$ in (4.7) and M_j in (4.8) are redefined by*

$$m_j^{(i)} := \min_{x \in S_j} P_j^{(i)}(x), \quad i = 1, \ldots, N; \quad M_j := \max_{x \in S_j}\left(\sum_{i=1}^{N} \tilde{P}_j^{(i)}(x)\right),$$

where S_j is the stencil (4.11) of Legendre-Gauss-Lobatto quadrature points for I_j. Let μ be as in (3.38). If the CFL condition

$$\alpha \lambda_n \le \mu \hat{w}_1, \quad \alpha := \max_j\{|S_{L,j+1/2}|, |S_{R,j+1/2}|\}, \tag{4.15}$$

is in effect and $\Phi_j^n \in \mathcal{D}_{\phi_{\max}}$, then $\Phi_j^{n+1} \in \mathcal{D}_{\phi_{\max}}$.

Proof. We use the marching formula (4.5) along with (4.12) and add and subtract $\mathcal{F}(\Phi_{j-1/2}^R, \Phi_{j+1/2}^L)$ to get

$$\begin{aligned}
\Phi_j^{n+1} &= \sum_{\alpha=2}^{G-1} \hat{w}_\alpha \bar{\boldsymbol{P}}_j(\hat{x}_j^\alpha) + \hat{w}_G\left(\Phi_{j+1/2}^L - \frac{\lambda_n}{\hat{w}_G}(\mathcal{F}(\Phi_{j+1/2}^L, \Phi_{j+1/2}^R) - \mathcal{F}(\Phi_{j-1/2}^R, \Phi_{j+1/2}^L))\right) \\
&\quad + \hat{w}_1\left(\Phi_{j-1/2}^R - \frac{\lambda_n}{\hat{w}_1}(\mathcal{F}(\Phi_{j-1/2}^R, \Phi_{j+1/2}^L) - \mathcal{F}(\Phi_{j-1/2}^L, \Phi_{j-1/2}^R))\right) \\
&= \sum_{\alpha=2}^{G-1} \hat{w}_\alpha \bar{\boldsymbol{P}}_j(\hat{x}_j^\alpha) + \hat{w}_G \mathcal{H}(\Phi_{j-1/2}^R, \Phi_{j+1/2}^L, \Phi_{j+1/2}^R) + \hat{w}_1 \mathcal{H}(\Phi_{j-1/2}^L, \Phi_{j-1/2}^R, \Phi_{j+1/2}^L),
\end{aligned}$$

where $\mathcal{H}(\cdot, \cdot, \cdot)$ is the three-point operator analyzed in Theorems 1-2. By Lemma 1 we know that $\bar{\boldsymbol{P}}_j(\hat{x}_j^\alpha) \in \mathcal{D}_{\phi_{\max}}$ for $j = 2, \ldots, G-1$, and Theorems 1-2, in conjunction with the CFL condition (4.15), guarantees that

$$\mathcal{H}(\Phi_{j-1/2}^R, \Phi_{j+1/2}^L, \Phi_{j+1/2}^R), \ \mathcal{H}(\Phi_{j-1/2}^L, \Phi_{j-1/2}^R, \Phi_{j+1/2}^L) \in \mathcal{D}_{\phi_{\max}}.$$

Consequently, Φ_j^{n+1} can be expressed as a convex combination of terms in $\mathcal{D}_{\phi_{\max}}$. This concludes the proof. $\qquad\square$

4.4. Accuracy of the limiter

We now adapt the ideas in [20, 40] to rigorously discuss the accuracy of the limiter (4.9). To this end, let us suppose that $\boldsymbol{P}_j(x)$ approximates a smooth solution $\Phi(x) = (\phi_1(x), \ldots, \phi_N(x))^{\mathrm{T}} \in \mathcal{D}_{\phi_{\max}}^{\delta}$, i.e., $\|\boldsymbol{P}_j(x) - \Phi(x)\| = O(\Delta x^{r+1})$ for any $x \in I_j$. Our goal is to show that limiting polynomials $\bar{\boldsymbol{P}}_j(x)$ given by (4.9) also satisfies $\|\bar{\boldsymbol{P}}_j(x) - \Phi(x)\| = O(\Delta x^{r+1})$ for any $x \in I_j$. First, we analyze the accuracy of the limiter (4.7). For a given i, we only discuss the case when $\tilde{P}_j^{(i)}(x)$ is not a constant polynomial. If $\theta_i = 1$, then $\tilde{P}_j^{(i)}(x) = P_j^{(i)}(x)$ and we have nothing to show. So, let us assume that

$$\theta_i = \frac{\phi_{i,j}^n - \delta}{\phi_{i,j}^n - m_j^{(i)}}. \tag{4.16}$$

We observe that

$$\tilde{P}_j^{(i)}(x) - P_j^{(i)}(x) = \theta_i(P_j^{(i)}(x) - \phi_{i,j}^n) + \phi_{i,j}^n - P_j^{(i)}(x) = (\theta_i - 1)(P_j^{(i)}(x) - \phi_{i,j}^n)$$

$$= \frac{m_j^{(i)} - \delta}{\phi_{i,j}^n - m_j^{(i)}}(P_j^{(i)}(x) - \phi_{i,j}^n) = (\delta - m_j^{(i)})\frac{\phi_{i,j}^n - P_j^{(i)}(x)}{\phi_{i,j}^n - m_j^{(i)}},$$

so we get

$$\left|\tilde{P}_j^{(i)}(x) - P_j^{(i)}(x)\right| \le \left|\delta - m_j^{(i)}\right|\left|\frac{\phi_{i,j}^n - P_j^{(i)}(x)}{\phi_{i,j}^n - m_j^{(i)}}\right|.$$

The assumption that θ_i given by (4.16) satisfies $\theta_i < 1$ implies that $\phi_{i,j}^n - \delta < \phi_{i,j}^n - m_j^{(i)}$, so we get $m_j^{(i)} < \delta$. So, if $x_*^{(i)} \in I_j$ is such that $\tilde{P}_j^{(i)}(x_*^{(i)}) = m_j^{(i)}$, then $\tilde{P}_j^{(i)}(x_*^{(i)}) = m_j^{(i)} < \delta \le \phi_i(x_*^{(i)})$. From this we get the bound

$$\left|\delta - m_j^{(i)}\right| \le \left|\phi_i(x_*^{(i)}) - \tilde{P}_j^{(i)}(x_*^{(i)})\right| \le \max_{x \in I_j}\left|\phi_i(x) - \tilde{P}_j^{(i)}(x)\right|.$$

Consequently, we get $\delta - m_j^{(i)} = O(\Delta x^{r+1})$. Thus, we only have to establish upper bounds for the scalar quantities

$$\left|\frac{\phi_{i,j}^n - P_j^{(i)}(x)}{\phi_{i,j}^n - m_j^{(i)}}\right|, \quad i = 1, \ldots, N,$$

which can be done by following [40, Appendix C]. We have shown that $\|\tilde{\boldsymbol{P}}_j(x) - \boldsymbol{P}_j(x)\| = O(\Delta x^{r+1})$ for any $x \in I_j$.

Now we address the limiter (4.9). For a given i, we assume that $\bar{P}_j^{(i)}(x)$ is not a constant polynomial. If $\hat{\theta} = 1$, then $\bar{P}_j^{(i)}(x) = \tilde{P}_j^{(i)}(x)$ and we have nothing to show. So, let us consider

$$\hat{\theta} = \frac{\phi_{\max} - \phi_j^n}{M_j - \phi_j^n}. \tag{4.17}$$

We observe that

$$\bar{P}_j^{(i)}(x) - \tilde{P}_j^{(i)}(x) = \hat{\theta}(\tilde{P}_j^{(i)}(x) - \phi_{i,j}^n) + \phi_{i,j}^n - \tilde{P}_j^{(i)}(x) = (\hat{\theta} - 1)(\tilde{P}_j^{(i)}(x) - \phi_{i,j}^n)$$

$$= \frac{\phi_{\max} - M_j}{M_j - \phi_j^n}(\tilde{P}_j^{(i)}(x) - \phi_{i,j}^n) = (\phi_{\max} - M_j)\frac{\tilde{P}_j^{(i)}(x) - \phi_{i,j}^n}{M_j - \phi_j^n},$$

so we obtain

$$\left|\bar{P}_j^{(i)}(x) - \tilde{P}_j^{(i)}(x)\right| \le \left|\phi_{\max} - M_j\right|\left|\frac{\tilde{P}_j^{(i)}(x) - \phi_{i,j}^n}{M_j - \phi_j^n}\right|.$$

16

In the same way as in the analysis of (4.7), we notice that the assumption that $\hat{\theta}$ given by (4.17) satisfies $\hat{\theta} < 1$ produces $\phi_{\max} - \phi_j^n < M_j - \phi_j^n$ which implies $M_j > \phi_{\max}$. So, if $x_* \in I_j$ is such that $\sum_{\ell=1}^N \tilde{P}_j^{(\ell)}(x_*) = M_j$, then we have

$$\phi(x_*) \leq \phi_{\max} < M_j = \sum_{\ell=1}^N \tilde{P}_j^{(\ell)}(x_*),$$

which implies the bound

$$\left| \phi_{\max} - M_j \right| \leq \left| \sum_{\ell=1}^N \tilde{P}_j^{(\ell)}(x_*) - \phi(x_*) \right| = \left| \sum_{\ell=1}^N \left(\tilde{P}_j^{(\ell)}(x_*) - \phi_\ell(x_*) \right) \right| = \left| \sum_{\ell=1}^N \left(\tilde{P}_j^{(\ell)}(x_*) - P_j^{(\ell)}(x_*) + P_j^{(\ell)}(x_*) - \phi_\ell(x_*) \right) \right|$$

$$\leq \sum_{\ell=1}^N \left| \tilde{P}_j^{(\ell)}(x_*) - P_j^{(\ell)}(x_*) \right| + \sum_{\ell=1}^N \left| P_j^{(\ell)}(x_*) - \phi_\ell(x_*) \right| \lesssim \left\| \tilde{P}_j(x_*) - P_j(x_*) \right\| + \left\| \tilde{P}_j(x_*) - \Phi(x_*) \right\| = O(\Delta x^{r+1}).$$

Thus, we get $M_j - \phi_{\max} = O(\Delta x^{r+1})$. In addition, we notice that

$$M_j - \phi_j^n \geq \sum_{\ell=1}^N (M_j^{(\ell)} - \phi_{\ell,j}^n) \geq M_j^{(i)} - \phi_{i,j}^n,$$

where $M_j^{(i)} = \max_{x \in I_j} \tilde{P}_j^{(i)}(x)$ for each $i = 1, \ldots, N$. Consequently, we arrive at the bound

$$\left| \frac{\tilde{P}_j^{(i)}(x) - \phi_{i,j}^n}{M_j - \phi_j^n} \right| \leq \left| \frac{\tilde{P}_j^{(i)}(x) - \phi_{i,j}^n}{M_j^{(i)} - \phi_{i,j}^n} \right|, \quad i = 1, \ldots, N.$$

Therefore, we only have to establish upper bounds for the scalar quantities

$$\left| \frac{\tilde{P}_j^{(i)}(x) - \phi_{i,j}^n}{M_j^{(i)} - \phi_{i,j}^n} \right|, \quad i = 1, \ldots, N,$$

which can be obtained by following again [40, Appendix C]. In this way, we have proved that

$$\left\| \bar{P}_j(x) - \tilde{P}_j(x) \right\| = O(\Delta x^{r+1}) \quad \text{for any } x \in I_j.$$

Finally, we obtain

$$\left\| \bar{P}_j(x) - \Phi(x) \right\| \leq \left\| \bar{P}_j(x) - \tilde{P}_j(x) \right\| + \left\| \tilde{P}_j(x) - P_j(x) \right\| + \left\| P_j(x) - \Phi_j(x) \right\| = O(\Delta x^{r+1}) \quad \text{for any } x \in I_j.$$

Remark 4. *Following [21, Section 5], we point out that the quantities $m_j^{(i)}$, $i = 1, \ldots, N$ and M_j can be computed in a less expensive way. For instance, if $i \in \{1, \ldots, N\}$ is fixed, one can use the Mean Value Theorem to get that*

$$P_j^{(i)}(\xi^{(i)}) = \sum_{\alpha=2}^{G-1} \frac{\hat{w}_\alpha}{1 - 2\hat{w}_1} P_j^{(i)}(\hat{x}_j^\alpha), \quad \text{for some } \xi^{(i)} \in I_j.$$

The convex combination $\phi_{i,j}^n = \sum_{\alpha=1}^G \hat{w}_\alpha P_j^{(i)}(\hat{x}_j^\alpha)$ implies $\phi_{i,j}^n = \hat{w}_1 P_j^{(i)}(x_{j-1/2}) + \hat{w}_G P_j^{(i)}(x_{j+1/2}) + (1 - 2\hat{w}_1) P_j^{(i)}(\xi^{(i)})$, from which we deduce that

$$P_j^{(i)}(\xi^{(i)}) = \frac{1}{1 - 2\hat{w}_1} \left(\phi_{i,j}^n - \hat{w}_1 P_j^{(i)}(x_{j-1/2}) - \hat{w}_G P_j^{(i)}(x_{j+1/2}) \right),$$

i.e. we can compute the value of $P_j^{(i)}(x)$ at $x = \xi^{(i)}$ even though the value of $\xi^{(i)}$ is unknown. Thus the minimum value of $P_j^{(i)}(x)$ over I_j is computed as

$$\widehat{m}_j^{(i)} = \min \left\{ P_j^{(i)}(\xi^{(i)}), P_j^{(i)}(x_{j-1/2}), P_j^{(i)}(x_{j+1/2}) \right\}, \quad i = 1, \ldots, N. \tag{4.18}$$

Analogously, for the case of the maximum M_j, we apply the Mean Value Theorem to the polynomial

$$Q_j(x) := \sum_{i=1}^{N} \tilde{P}_j^{(i)}(x),$$

to get a value $\xi \in I_j$ such that

$$Q_j(\xi) = \sum_{\alpha=2}^{G-1} \frac{\hat{w}_\alpha}{1 - 2\hat{w}_1} Q_j(\hat{x}_j^\alpha).$$

One can also notice that

$$\phi_j^n = \sum_{i=1}^{N} \phi_{i,j}^n = \sum_{i=1}^{N} \frac{1}{\Delta x} \int_{I_j} \tilde{P}_j^{(i)}(x) \, dx = \sum_{i=1}^{N} \sum_{\alpha=1}^{G} \hat{w}_\alpha \tilde{P}_j^{(i)}(\hat{x}_j^\alpha) = \sum_{\alpha=1}^{G} \hat{w}_\alpha Q_j(\hat{x}_j^\alpha),$$

hence we can compute $Q_j(\xi)$ by the formula

$$Q_j(\xi) = \frac{1}{1 - 2\hat{w}_1} \Big(\phi_j^n - \hat{w}_1 Q_j(x_{j-1/2}) - \hat{w}_G Q_j(x_{j+1/2}) \Big).$$

Consequently, the maximum value of $Q_j(x)$ over I_j is computed as

$$\widehat{M}_j = \max \Big\{ Q_j(\xi), Q_j(x_{j-1/2}), Q_j(x_{j+1/2}) \Big\}. \tag{4.19}$$

So, in the numerical computations we actually use the values:

$$\theta_i := \min \left\{ \frac{\phi_{i,j}^n - \delta}{\phi_{i,j}^n - \widehat{m}_j^{(i)}}, 1 \right\}, \ i = 1, \dots, N, \quad and \quad \hat{\theta} := \min \left\{ \left| \frac{\phi_{\max} - \phi_j^n}{\widehat{M}_j - \phi_j^n} \right|, 1 \right\}. \tag{4.20}$$

First we observe that

$$\phi_{i,j}^n = \hat{w}_1 P_j^{(i)}(x_{j-1/2}) + \hat{w}_G P_j^{(i)}(x_{j+1/2}) + (1 - 2\hat{w}_1) P_j^{(i)}(\xi^{(i)}) \geq \hat{w}_1 \widehat{m}_j^{(i)} + \hat{w}_G \widehat{m}_j^{(i)} + (1 - 2\hat{w}_1) \widehat{m}_j^{(i)} = \widehat{m}_j^{(i)},$$

thus, $\theta_i \in [0, 1]$, $i = 1, \dots, N$. In addition, we have that

$$P_j^{(i)}(\xi^{(i)}) = \sum_{\alpha=2}^{G-1} \frac{\hat{w}_\alpha}{1 - 2\hat{w}_1} P_j^{(i)}(\hat{x}_j^\alpha) \geq \frac{m_j^{(i)}}{1 - 2\hat{w}_1} \sum_{\alpha=2}^{G-1} \hat{w}_\alpha = \frac{m_j^{(i)}}{1 - 2\hat{w}_1} (1 - 2\hat{w}_1) = m_j^{(i)},$$

hence $m_j^{(i)} \leq \widehat{m}_j^{(i)}$. In this way we get that

$$\frac{\phi_{i,j}^n - \delta}{\phi_{i,j}^n - m_j^{(i)}} \leq \frac{\phi_{i,j}^n - \delta}{\phi_{i,j}^n - \widehat{m}_j^{(i)}}, \quad i = 1, \dots, N.$$

Analogously, we notice that $\widehat{M}_j \leq M_j$ and therefore

$$\left| \frac{\phi_{\max} - \phi_j^n}{M_j - \phi_j^n} \right| \leq \left| \frac{\phi_{\max} - \phi_j^n}{\widehat{M}_j - \phi_j^n} \right|.$$

So, the limiters with the values (4.18) and (4.19) are more relaxed than (4.7) and (4.8), respectively. Therefore the analysis of accuracy performed above is still valid.

4.5. Time discretization

High-order time integration is required to ensure the appropriate order of convergence of the method. In this work, a strong-stability preserving (SSP) third-order TVD Runge-Kutta time discretization approach is used [49]. This time stepping method could be described as follows. Assume that Φ^n is the vector of approximate solutions of $\Phi' = \mathcal{L}(\Phi)$ at $t = t_n$. Then the approximate values Φ^{n+1} associated with $t_{n+1} = t_n + \Delta t$ are calculated by

$$
\begin{aligned}
\Phi^{(1)} &= \Phi^n + \Delta t \mathcal{L}(\Phi^n), \\
\Phi^{(2)} &= \frac{3}{4}\Phi^n + \frac{1}{4}\Phi^{(1)} + \frac{1}{4}\Delta t \mathcal{L}(\Phi^{(1)}), \\
\Phi^{n+1} &= \frac{1}{3}\Phi^n + \frac{2}{3}\Phi^{(2)} + \frac{2}{3}\Delta t \mathcal{L}(\Phi^{(2)}).
\end{aligned}
\tag{4.21}
$$

We refer to (4.21) as SSPRK (3,3). The SSP time discretization methods are widely used for hyperbolic PDE because they preserve nonlinear stability properties necessary for problems with non-smooth solutions. On the other hand, due to convexity, the intermediate stages of the SSPRK methods have SSP properties (i.e., $\|\Phi^n\| \leq \|\Phi^{n-1}\|$ for the internal stages). Consequently, the present finite volume WENO scheme with this time discretization will still satisfy the maximum principle. Since it is necessary to evaluate three times the operator $\mathcal{L}(\cdot)$ to advance one time step, the effective SSP coefficient for SSPRK (3,3) the method (which is defined as in [10]; namely the SSP coefficient of the method divided by the number of stages) equals $1/3$.

To satisfy the CFL condition (4.15) the time step Δt is computed adaptively for each time step n. More specifically, the solution Φ^{n+1} at $t_{n+1} = t_n + \Delta t$ is calculated from Φ^n by using $\Delta t = \mu(\hat{w}_1 \Delta x / \alpha)$, where μ is given by (3.38).

5. Numerical examples

5.1. Preliminaries

We discretize the domain $[0, L] \times [0, T]$ as outlined in Section 3.1. For the MLB model, we employ the first-order LLF flux given by (3.4) and the HLL flux, defined by (3.22). For the MCLWR model, we only use the LLF method. For computing the nonlinear weights (4.1) in the WENO reconstruction procedure, we have set $p = 2$ in all numerical test and we have used $\varepsilon = \Delta x^2$ and $\varepsilon = 10^{-6}$ in the first example (accuracy test) to show the robustness of the WENO scheme for both choices of the parameters ε while in the rest of examples we use $\varepsilon = \Delta x^2$. The remaining parameters of the reconstructions are taken as usual (see [50, 51]). In the first example, we compare numerical results obtained by the invariant region preserving WENO schemes of orders 3 and 5. For the rest of examples, we limit ourselves to third-order WENO reconstructions. We denote by "IRP-LFW-3" and "IRP-HLLW-3" the LLF and HLL methods, respectively, with third-order IRP WENO reconstructions. Analogously, "IRP-LFW-5" and "IRP-HLLW-5" denote the respective fifth-order versions.

For comparison purposes, we compute reference solutions for numerical tests by the IRP-WENO-5 scheme with $M_{\text{ref}} = 12800$ in Example 1, by IRP-HLLW-3 with $M_{\text{ref}} = 6400$ in Examples 2 and 3, and by IRP-LFW-3 with $M_{\text{ref}} = 6400$ in Examples 4 and 5. As in [15, 18], we compute approximate L^1 errors at different times for each scheme as follows. We denote by $(\phi_{i,j}^n(t))_{j=1}^M$ and $(\phi_{i,j}^{\text{ref}}(t))_{j=1}^{M_{\text{ref}}}$ the numerical solution for the i-th component at time t calculated with M and M_{ref} cells, respectively. We compute $\tilde{\phi}_{i,j}^{\text{ref}}(t)$, for $j = 1, \ldots, M$, by

$$
\tilde{\phi}_{i,j}^{\text{ref}}(t) = \frac{1}{R} \sum_{k=1}^{R} \phi_{i,R(j-1)+k}^{\text{ref}}(t), \quad R = M_{\text{ref}}/M.
$$

The total approximate L^1 error of the numerical solution on the M-cell grid at time T is then given by

$$
e_M^{\text{tot}}(t) := \frac{1}{M} \sum_{i=1}^{N} \sum_{j=1}^{M} \left| \tilde{\phi}_{i,j}^{\text{ref}}(t) - \phi_{i,j}^M(t) \right|.
\tag{5.1}
$$

We may then calculate a numerical order of convergence from $e_M^{\text{tot}}(t)$ and $e_{2M}^{\text{tot}}(t)$ by

$$
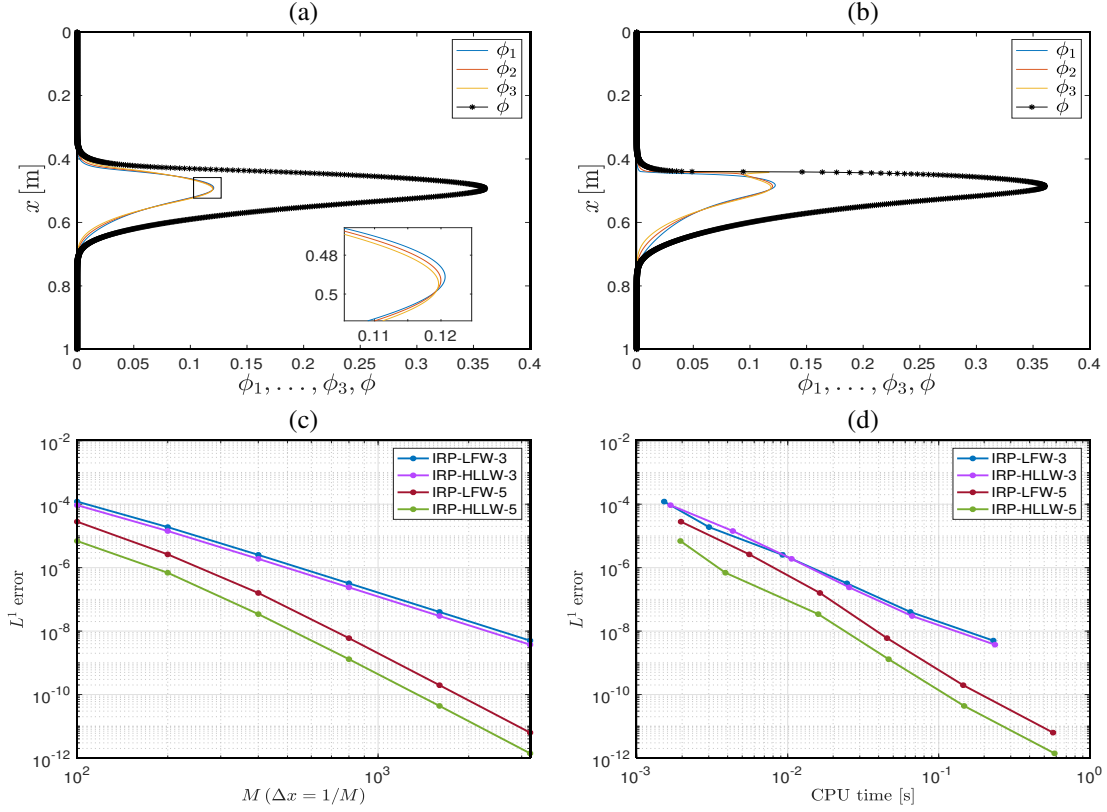\theta_M(t) := \log_2 \left(e_M^{\text{tot}}(t)/e_{2M}^{\text{tot}}(t) \right).
\tag{5.2}
$$

19

Figure 1: Example 1 (MLB Model, $N = 3$): numerical results obtained by scheme IRP-HLLW-5 with $M = 1600$ at simulated time (a) $T = 5\,\mathrm{s}$, (b) $T = 10\,\mathrm{s}$, (c) approximate L^1 errors for all schemes tested as function of M, (d) efficiency plot obtained for discretization levels $\Delta x = 1/M$ with $M = 100, 200, 400, 800,$ and 1600.

In order to study the effect of the limiters (4.7) and (4.8), we compute the minimum values of the numerical solution in space and time for each component and the maximum values of the numerical solution in space and time for the total concentration with and without the limiters, i.e. we compute:

$$\underline{\phi}_{,i} := \min_{(j,n)\in\mathbb{Z}_M\times\mathbb{Z}_T}\{\phi^n_{i,j}\}, \quad i = 1,\ldots,N, \quad \text{and} \quad \overline{\phi} := \max_{(j,n)\in\mathbb{Z}_M\times\mathbb{Z}_T}\{\phi^n_j\},$$

where $\mathbb{Z}_T := \{0,\ldots,N_T\}$.

5.2. Example 1: MLB model, $N = 3$, numerical order of accuracy

In this example, we consider an experiment performed in [52] to verify numerically the convergence rate of the IRP-LFW-3, IRP-HLLW-3, IRP-LFW-5, and IRP-HLLW-5 numerical schemes. We employ the MLB model introduced in Section 2 with $N = 3$ species having normalized squared particle sizes $\delta = (1, 0.8, 0.6)^{\mathrm{T}}$ with density $\rho_s = 2790\,\mathrm{kg/m}^3$ and vessel height $L = 1\,\mathrm{m}$. The maximum total concentration is $\phi_{\max} = 0.66$. The hindered settling factor $V(\phi)$ is chosen according to (2.7) with the exponent $n_{\mathrm{RZ}} = 4.7$. The remaining parameters are $g = 9.81\,\mathrm{m/s}^2$, $\mu_{\mathrm{f}} = 0.02416\,\mathrm{Pas}$ and $\rho_{\mathrm{f}} = 1208\,\mathrm{kg/m}^3$. We choose a smooth initial concentration profile given by $\Phi_0(x) = 0.12\exp(-200(x - 0.5)^2)(0.12, 0.12, 0.12)^{\mathrm{T}}$. We compute approximate solutions with $\Delta x = L/M$, and $M = 100 \cdot 2^\ell$, $\ell = 0\ldots,5$, and a fixed time step $\Delta t = 50\Delta x$, for the third-order method. Since the order of TVD Runge-Kutta time step solver is 3, in the case of fifth-order schemes, we use a time step Δt such that $(\Delta t)^3$ is maintained proportional to Δx^5, i.e we just set $\Delta t \propto \Delta x^{5/3}$, in order to get the correct convergence rate. Figure 1 shows the numerical results for $M = 1600$ at $T = 5\,\mathrm{s}$ (before shock formation, when the solution is still smooth) and for $T = 10\,\mathrm{s}$ (after shock formation).

Table 1: Example 1 (MLB model, $N = 3$): L^1 errors and numerical order for IRP-LFW-3, IRP-HLLW-3, IRP-LFW-5, and IRP-HLLW-5 schemes applied to smooth initial conditions for $T = 5$ s (before shock formation) and $T = 10$ s (after shock formation) for values of $\varepsilon = \Delta x^2$ and $\varepsilon = 10^{-6}$. The reference solution is computed by IRP-HLLW-5 with $M_{\text{ref}} = 12800$.

	$\varepsilon = \Delta x^2$											
M	e_M^{tot}	θ_M	cpu [s]	e_M^{tot}	θ_M	cpu [s]	e_M^{tot}	θ_M	cpu [s]	e_M^{tot}	θ_M	cpu [s]
	IRP-LFW-3, $T = 5$ s			IRP-LFW-3, $T = 10$ s			IRP-HLLW-3, $T = 5$ s			IRP-HLLW-3, $T = 10$ s		
100	1.21e-04	–	1.52e-03	7.90e-04	—	3.18e-03	9.32e-05	—	1.67e-03	6.73e-04	—	2.61e-03
200	1.90e-05	2.6	3.01e-03	3.51e-04	1.2	7.06e-03	1.43e-05	2.7	4.33e-03	2.95e-04	1.2	6.21e-03
400	2.53e-06	2.9	9.25e-03	1.58e-04	1.1	1.64e-02	1.89e-06	2.9	1.06e-02	1.30e-04	1.2	1.56e-02
800	3.2e-07	3.0	2.47e-02	6.42e-05	1.3	4.08e-02	2.39e-07	3.0	2.55e-02	5.08e-05	1.3	4.10e-02
1600	4.01e-08	3.0	6.50e-02	2.39e-05	1.4	0.12	2.99e-08	3.0	6.67-02	1.81e-05	1.5	0.12
3200	5.01e-09	3.0	0.23	1.57e-05	0.6	0.47	3.73e-09	3.0	0.24	1.28e-05	0.5	0.48
	IRP-LFW-5, $T = 5$ s			IRP-LFW-5, $T = 10$ s			IRP-HLLW-5, $T = 5$ s			IRP-HLLW-5, $T = 10$ s		
100	2.81e-05	—	1.96e-03	5.95e-04	—	6.16e-03	6.92e-06	—	1.95e-03	2.38e-04	—	4.77e-03
200	2.62e-06	3.4	5.57e-03	2.92e-04	1.0	1.31e-02	6.9e-06	3.3	3.87e-03	1.09e-04	1.1	1.32e-02
400	1.59e-07	4.0	1.63e-02	1.20e-04	1.3	2.99e-02	3.43e-08	4.3	1.59e-02	4.80e-05	1.2	3.02e-02
800	6.0e-09	4.7	4.55e-02	4.21e-05	1.5	7.85e-02	1.3e-09	4.7	4.66e-02	1.74e-05	1.5	8.07e-02
1600	1.97e-10	4.9	0.14	1.18e-05	1.8	0.29	4.37e-11	4.9	0.15	5.27e-06	1.7	0.29
3200	6.29e-12	5.0	0.57	9.94e-06	0.2	1.14	1.4e-12	5.0	0.58	5.15e-06	0.0	1.15
	$\varepsilon = 10^{-6}$											
M	e_M^{tot}	θ_M	cpu [s]	e_M^{tot}	θ_M	cpu [s]	e_M^{tot}	θ_M	cpu [s]	e_M^{tot}	θ_M	cpu [s]
	IRP-LFW-3, $T = 5$ s			IRP-LFW-3, $T = 10$ s			IRP-HLLW-3, $T = 5$ s			IRP-HLLW-3, $T = 10$ s		
100	2.96e-04	—	1.08e-03	1.04e-03	—	3.17e-03	2.2e-04	—	1.37e-03	8.63e-04	—	3.09e-03
200	5.03e-05	2.7	3.89e-03	4.29e-04	1.3	7.23e-03	3.72e-05	2.6	3.39e-03	3.54e-04	1.3	7.23e-03
400	4.33e-06	3.5	1.03e-02	1.68e-04	1.4	1.65e-02	3.12e-06	3.6	9.27e-03	1.37e-04	1.4	1.64e-02
800	3.57e-07	3.6	2.55e-02	6.48e-05	1.4	4.1e-02	2.64e-07	3.5	2.48e-02	5.12e-05	1.4	4.15e-02
1600	3.36e-08	3.4	6.55e-02	2.33e-05	1.5	0.12	2.55e-08	3.4	6.64e-02	1.77e-05	1.5	0.12
3200	3.75e-09	3.2	0.23	1.51e-05	0.6	0.47	2.89e-09	3.1	0.24	1.23e-05	0.5	0.48
	IRP-LFW-5, $T = 5$ s			IRP-LFW-5, $T = 10$ s			IRP-HLLW-5, $T = 5$ s			IRP-HLLW-5, $T = 10$ s		
100	2.81e-05	—	2.07e-03	6.58e-04	—	4e-03	5.75e-06	—	2.8e-03	2.68e-04	—	4.58e-03
200	2.62e-06	3.4	8.18e-03	3.1e-04	1.1	8.67e-03	6.86e-07	3.1	7.13e-03	1.15e-04	1.2	1.02e-02
400	1.64e-07	4.0	1.08e-02	1.24e-04	1.3	2.06e-02	3.55e-08	4.3	1.83e-02	4.89e-05	1.2	2.17e-02
800	6.06e-09	4.8	4.37e-02	4.24e-05	1.5	9.56e-02	1.32e-09	4.7	4.68e-02	1.75e-05	1.5	9.01e-02
1600	1.91e-10	5.0	0.17	1.18e-05	1.8	0.38	4.28e-11	5.0	0.14	5.23e-06	1.7	0.34
3200	5.76e-12	5.1	0.63	9.84e-06	0.3	1.45	1.33e-12	5.0	0.58	5.1e-06	0.0	1.44

The approximate L^1 errors $e_M^{\text{tot}}(T)$ defined by (5.1) and their corresponding numerical orders $\theta_M(T)$ given by (5.2) are displayed in Table 1 at times $T = 5$ s and $T = 10$ s for both schemes. The reference solution is computed with $M_{\text{ref}} = 12800$ cells by using the fifth-order scheme IRP-HLLW-5. The behavior of $\theta_M(5)$ for increasing values of M confirms third-order convergence for smooth solutions for IRP-LFW-3, IRP-HLLW-3, and fifth order for schemes IRP-LFW-5, IRP-HLLW-5. The results for $T = 10$ s indicate that accuracy is reduced to first order when shocks are present, as expected.

5.3. Example 2: MLB model, $N = 2$

This example corresponds to $N = 2$ species with density $\rho_s = 2790$ kg/m^3 and different diameters $D_1 = 4.96 \times 10^{-4}$ m and $D_2 = 1.25 \times 10^{-4}$ m, such that $\boldsymbol{\delta} = (1, 0.063)^{\text{T}}$. The (unnormalized) depth of the vessel in the original experiment is $L = 0.3$ m [53]. The maximum total concentration is $\phi_{\max} = 0.6$, and the initial concentrations are $\Phi_0(x) = (0.2, 0.05)^{\text{T}}$. The remaining parameters are taken as in Example 1. The well-known solution of Example 2 has been used as a test case for a variety of methods [14, 15, 18]. For comparison purposes, we calculate numerical solutions for a sequence of spatial discretizations $\Delta x = L/M$ with IRP-LFW-3 and IRP-HLLW-3 schemes and compare the solutions with a reference solution with $M = M_{\text{ref}} = 6400$ obtained by the IRP-HLLW-3 scheme. The reference

Table 2: Example 1 (MLB model, $N = 3$): minimum of the solutions $\phi_{i,j}^n$, $i = 1, \ldots, 3$, and maximum of the solution ϕ_j^n obtained by schemes LFW-3, LFW-5 (without limiters) and IRP-LFW-3, IRP-LFW-5 (with limiters) until specified times T.

M	$\underline{\phi}_{,1}$	$\underline{\phi}_{,2}$	$\underline{\phi}_{,3}$	$\overline{\phi}$	$\underline{\phi}_{,1}$	$\underline{\phi}_{,2}$	$\underline{\phi}_{,3}$	$\overline{\phi}$
	LFW-3, $T = 10$ s				IRP-LFW-3, $T = 10$ s			
100	-1.846e-04	-8.838e-10	-4.313e-10	0.3586	7.32e-23	7.32e-23	7.32e-23	0.3586
200	1.659e-23	1.651e-23	1.595e-23	0.3598	3.969e-23	3.969e-23	3.969e-23	0.3598
400	2.203e-23	2.226e-23	2.258e-23	0.3603	3.002e-23	3.002e-23	3.002e-23	0.3603
800	2.293e-23	2.307e-23	2.327e-23	0.3603	2.629e-23	2.629e-23	2.629e-23	0.3603
1600	2.307e-23	2.314e-23	2.324e-23	0.3604	2.465e-23	2.465e-23	2.465e-23	0.3604
	LFW-5, $T = 10$ s				IRP-LFW-5, $T = 10$ s			
100	-1.515e-07	5.313e-23	5.313e-23	0.3597	5.352e-23	7.32e-23	7.32e-23	0.3596
200	2.785e-23	2.789e-23	2.788e-23	0.3601	2.271e-23	3.013e-23	3.969e-23	0.3601
400	2.456e-23	2.462e-23	2.469e-23	0.3603	2.585e-23	2.703e-23	2.852e-23	0.3603
800	2.374e-23	2.378e-23	2.382e-23	0.3603	2.475e-23	2.5e-23	2.547e-23	0.3603
1600	2.341e-23	2.343e-23	2.345e-23	0.3604	2.394e-23	2.405e-23	2.424e-23	0.3604

Table 3: Example 2 (MLB model, $N = 2$): L^1 errors, numerical order, and CPU time (seconds) for IRP-LFW-3 and IRP-HLLW-3 schemes at $T = 50$ s and $T = 300$ s. The reference solution is computed by IRP-HLLW-3 with $M_{\text{ref}} = 6400$.

M	e_M^{tot}	θ_M	cpu [s]	e_M^{tot}	θ_M	cpu [s]	e_M^{tot}	θ_M	cpu [s]	e_M^{tot}	θ_M	cpu [s]
	IRP-LFW-3, $T = 50$ s			IRP-LFW-3, $T = 300$ s			IRP-HLLW-3, $T = 50$ s			IRP-HLLW-3, $T = 300$ s		
100	6.56e-03	—	3.89e-02	9.50e-03	—	1.23e-01	4.78e-03	—	5.99e-02	4.93e-03	—	2.08e-01
200	3.83e-03	0.7	6.98e-02	4.79e-03	0.9	3.54e-01	2.83e-03	0.7	1.26e-01	2.10e-03	1.2	6.67e-01
400	2.05e-03	0.9	2.33e-01	2.35e-03	1.0	1.36	1.51e-03	0.9	5.04e-01	9.31e-04	1.1	2.59
800	1.02e-03	1.0	0.95e-01	9.69e-04	1.2	5.56	7.34e-04	1.0	2.04	4.59e-04	1.0	10.6
1600	4.67e-04	1.1	3.83	5.39e-04	0.8	21.8	3.15e-04	1.2	8.08	2.44e-04	0.9	41.7

solution is shown in Figures 2 and 3 for the simulated times $T = 50$ s and $T = 300$ s, respectively. On the other hand, we plot the solutions of the total concentration ϕ with $M = 2^\ell \cdot 100$, $\ell = 0, 1, \ldots, 3$ and the reference solution computed with $M = 6400$ mesh points in Figure 4.

In Table 3 we show approximate L^1 errors and CPU times for both schemes at two selected simulated times, these approximate errors are computed by (5.1) and we observe the convergence of both methods. The minimum values $\underline{\phi}_{,i}$ for $i = 1, 2$ and the maximum value $\overline{\phi}$, with and without the limiters are presented in Table 4. In the case of schemes without limiters we observe some negative values of $\underline{\phi}_{,i}$ and some values of $\overline{\phi}$ greater than $\phi_{\max}$ due to overshoots present in the numerical solution, see for example Figure 3 (d), while in the case of schemes with limiters the numerical solution belongs to $\mathcal{D}_{\phi_{\max}}$, as expected.

5.4. Example 3: MLB model, $N = 4$

In this example we consider $N = 4$ particle sizes with $D_1 = 4.96 \times 10^{-4}$ m, the rest of diameters D_i, $i = 2, 3, 4$ are chosen such that $\delta = (1, 0.8, 0.6, 0.4)^{\mathrm{T}}$ and we set $\Phi_0(x) = (0.05, 0.05, 0.05, 0.05)^{\mathrm{T}}$. The other parameters are as in Example 2. This example goes back to Greenspan and Ungarish [54], and was solved numerically in [55] with the slightly different hindered settling factor $V(\phi) = (1 - (5/3)\phi)^{2.7}$. The reference solution is shown in Figures 5 and 6 for the simulated times $T = 50$ s and $T = 300$ s, respectively. In Table 5 we show approximate L^1 errors and CPU times for both schemes at two selected simulated times and we observe the convergence of both methods. These approximate errors are computed by (5.1). The minimum values $\underline{\phi}_{,i}$ for $i = 1, \ldots, 4$ and the maximum value $\overline{\phi}$, with and without the limiters are presented in Table 6. In the case of schemes without limiters we observe some negative values of $\underline{\phi}_{,i}$ and some values of $\overline{\phi}$ greater than $\phi_{\max}$ due to overshoots present in the numerical solution, see for example Figure 6(d), while in the case of schemes with limiters the numerical solution belongs to $\mathcal{D}_{\phi_{\max}}$, as expected.
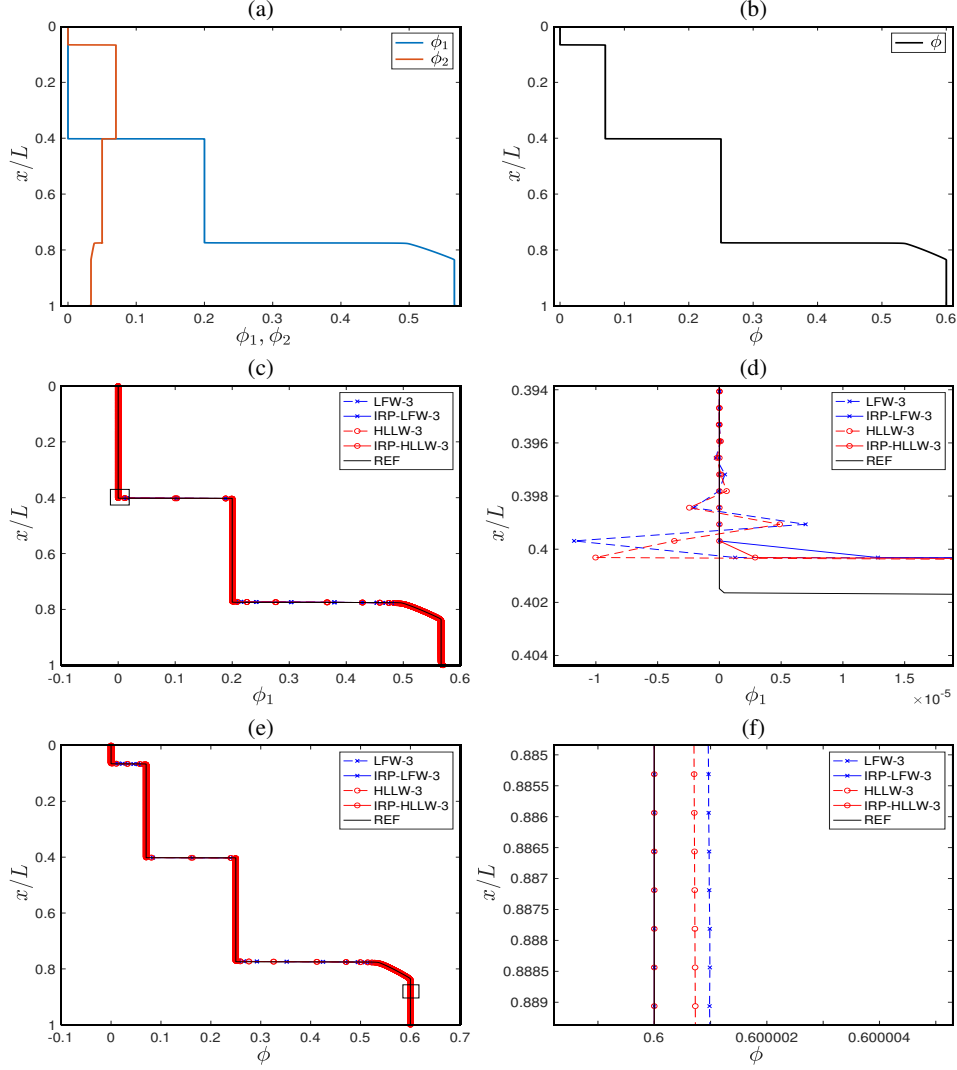
Figure 2: Example 2 (MLB model, $N = 2$): reference solution for (a) ϕ_1, ϕ_2 and (b) ϕ at $T = 50\,\mathrm{s}$ computed by scheme IRP-HLLW-3 with $M_{\mathrm{ref}} = 6400$, and comparison of schemes for (c) ϕ_1, (d) enlarged view of (c), (e) ϕ, and (f) enlarged view of (e) at $T = 50\,\mathrm{s}$ with $M = 1600$.

5.5. Example 4: MCLWR model, $N = 3$

We now study the MCLWR model on a road of length $L = 5$ mi (mi stands for miles) with $N = 3$ driver classes associated with $\beta_1 = 60\,\mathrm{mi/h}$, $\beta_2 = 55\,\mathrm{mi/h}$, and $\beta_3 = 50\,\mathrm{mi/h}$. We employ the Dick–Greenberg model (2.1) with $\phi_{\max} = 1$ and choose (as in [52]) $\phi_{\mathrm{c}} = \exp(-7/e) \approx 0.076142$. The velocity is then given by

$$\begin{cases} v(\phi) = 1, \ v'(\phi) = 0 & \text{for } 0 \le \phi \le \phi_{\mathrm{c}} = \exp(-1/C) \approx 0.076142, \\ v(\phi) = -C\ln(\phi), \ v'(\phi) = -C/\phi & \text{for } \phi_{\mathrm{c}} < \phi < 1. \end{cases}$$
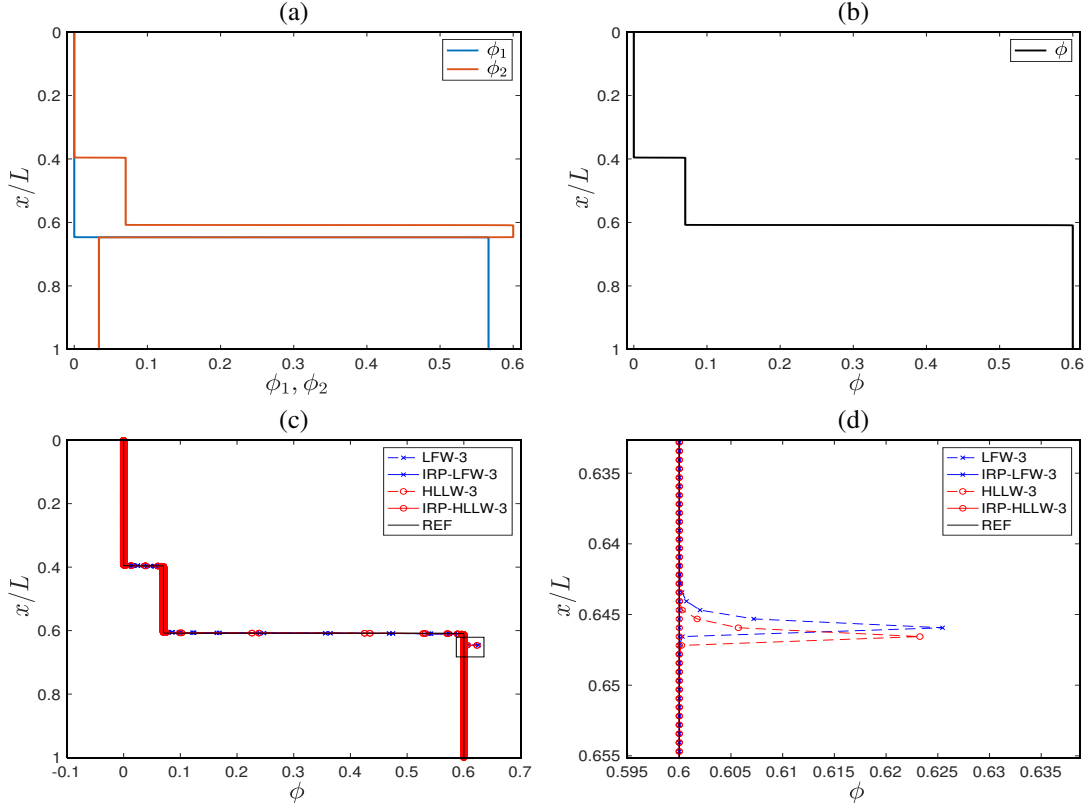
23

Figure 3: Example 2 (MLB model, $N = 2$): reference solution for (a) ϕ_1, ϕ_2 and (b) ϕ at $T = 300$ s computed by scheme IRP-HLLW-3 with $M_{\mathrm{ref}} = 6400$, and (c) comparison of schemes for ϕ_1, (d) enlarged view of (c), at $T = 300$ s with $M = 1600$.

The initial density distribution is given by $\Phi_0(x) = p(x)(0.25, 0.4, 0.35)^{\mathrm{T}}$, where p describes an isolated platoon on $1 \leq x \leq 2$ followed by a constant maximum density function for $x \geq 4$, i.e.,

$$
p(x) := \begin{cases}
10(x - 1) & \text{for } 1 \leq x \leq 1.1, \\
1 & \text{for } 1.1 \leq x \leq 1.9, \\
-10(x - 2) & \text{for } 1.9 \leq x \leq 2, \\
1 & \text{for } x \geq 4, \\
0 & \text{otherwise.}
\end{cases}
$$

For this particular case we use zero flux boundary conditions in order to obtain a steady state solution. The reference solution is shown in Figure 7 (a)-(b) and Figure 8 (a)-(b), for the simulated times $T = 0.05$ h and $T = 0.5$ h, respectively. In Table 7 we show approximate L^1 errors and CPU times for the scheme at the two selected simulated times and we observe convergence of the method. These approximate errors are computed by (5.1). In the case of the scheme without limiters we observe some negative values of $\underline{\phi}_{,i}$ and some values of $\overline{\phi}$ greater than $\phi_{\max}$ due to overshoots present in the numerical solution, see for instance Figures 8(c) and (d).

5.6. Example 5: Daganzo's test, $N = 4$

In this subsection, we study a test that Daganzo suggested in [56]. The parameters and boundary conditions are the same as in Example 4 with densities $\beta_1 = 60$ mi/h , $\beta_2 = 55$ mi/h , $\beta_3 = 50$ mi/h , and $\beta_4 = 45$ mi/h . In order to conduct a multiclass test that is appropriate for this scenario, we follow the ideas of Bürger et. al in [13] and we
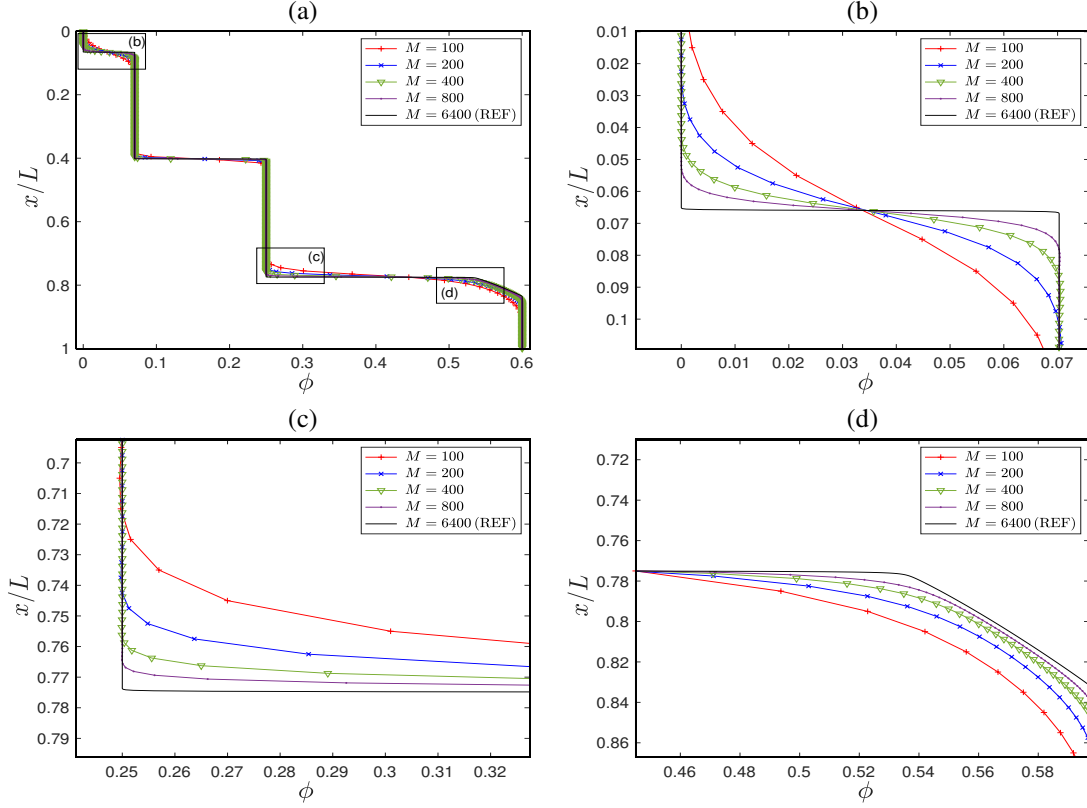
24

Figure 4: Example 2 (MLB model, $N = 2$): (a) comparison of the numerical solutions for ϕ at $T = 50\,\text{s}$ computed by IRP-HLLW-3 with various step sizes, (b)–(d) enlarged views of (a).

consider the initial condition

$$\Phi(x, 0) = \begin{cases} \Phi_{\text{L}} & \text{for } x < L/2, \\ \Phi_{\text{R}} & \text{for } x \geq L/2, \end{cases}$$

where $\Phi_{\text{L}} = (0, 0, 0, 0)^{\text{T}}$ and $\Phi_{\text{R}} = (0.25, 0.25, 0.25, 0.25)^{\text{T}}$. This density distribution should be a stationary solution for the model. The reference solution is shown in Figures 9(a) and (b) for the simulated time $T = 0.5\,\text{h}$. The minimum values $\underline{\phi}_i$ for $i = 1, \ldots, 4$ and the maximum value $\bar{\phi}$, with and without the limiters are presented in Table 9. See also Figures 9(c)–(f).

6. Conclusions

In this work, we have designed high-order finite volume numerical schemes for multiclass kinematic flow problems, including polydisperse sedimentation and multiclass vehicular traffic models, whose numerical solution preserves an invariant region which corresponds to the space $\mathcal{D}_{\phi_{\text{max}}}$ of physically relevant solutions of the model. The first contribution of the paper is the proof that first order schemes with the LLF numerical flux given by (3.4) and the HLL numerical flux given by (3.22) are invariant region preserving (IRP) for the MLB polydisperse sedimentation model, under some appropriate CFL conditions (3.10) and (3.25), respectively. The key part of the proof was to assume the conditions (2.9) and to consider the slightly lower bound for the eigenvalues of the model given by (3.8). We also proof that these schemes are IRP for MCLWR model under the assumptions (2.3). One can also use the HW scheme (Scheme 4 in [12]) which satisfies Theorem 1 but happens to be too dissipative. Next, by considering a component-wise WENO reconstruction, we use a modification of Zhang and Shu's scaling limiter [8] which consists

25

Table 4: Example 2 (MLB model, $N = 2$): minimum of the solutions $\underline{\phi}^n_{i,j}$, $i = 1, 2$, and maximum of the solution $\overline{\phi}^n_j$ obtained by schemes LFW-3 (without limiters), IRP-LFW-3 (with limiters), HLLW-3 (without limiters), and IRP-HLLW-3 (with limiters) until specified times T.

M	$\underline{\phi}_{,1}$	$\underline{\phi}_{,2}$	$\overline{\phi}$	$\underline{\phi}_{,1}$	$\underline{\phi}_{,2}$	$\overline{\phi}$
	LFW-3, $T = 50$ s			IRP-LFW-3, $T = 50$ s		
100	-4.122e-004	9.755e-004	0.600045	2.056e-025	9.763e-004	0.600000
200	-2.043e-004	-2.236e-004	0.600026	1.908e-039	7.263e-013	0.600000
400	-1.013e-004	-2.503e-004	0.600016	1.442e-067	3.434e-013	0.600000
800	-5.030e-005	-1.365e-004	0.600010	7.517e-124	1.163e-013	0.600000
1600	-2.513e-005	-6.839e-005	0.600010	2.073e-236	2.049e-014	0.600000
	LFW-3, $T = 300$ s			IRP-LFW-3, $T = 300$ s		
100	-4.130e-004	-1.076e-003	0.618048	1.061e-046	1.648e-013	0.600000
200	-2.047e-004	-5.425e-004	0.654617	3.884e-083	4.135e-014	0.600000
400	-1.013e-004	-2.724e-004	0.637268	1.829e-155	3.924e-015	0.600000
800	-5.035e-005	-1.365e-004	0.650888	4.012e-300	5.758e-017	0.600000
1600	-2.513e-005	-6.839e-005	0.625597	1.729e-322	2.228e-020	0.600000
	HLLW-3, $T = 50$ s			IRP-HLLW-3, $T = 50$ s		
100	-4.032e-004	-2.881e-004	0.600047	1.767e-025	2.279e-09	0.600000
200	-1.994e-004	-2.598e-004	0.600029	1.623e-039	3.968e-014	0.600000
400	-9.873e-005	-1.308e-004	0.600020	1.222e-067	4.873e-017	0.600000
800	-4.895e-005	-6.560e-005	0.600024	6.608e-124	3.263e-022	0.600000
1600	-2.442e-005	-3.288e-005	0.600034	1.771e-236	4.069e-032	0.600000
	HLLW-3, $T = 300$ s			IRP-HLLW-3, $T = 300$ s		
100	-4.032e-004	-5.196e-004	0.656865	3.090e-047	7.971e-020	0.600000
200	-1.991e-004	-2.609e-004	0.666836	3.593e-083	2.388e-027	0.600000
400	-9.873e-005	-1.308e-004	0.642500	1.635e-155	5.389e-042	0.600000
800	-4.895e-005	-6.560e-005	0.646103	3.455e-300	6.799e-071	0.600000
1600	-2.442e-005	-3.288e-005	0.623364	2.734e-322	2.678e-128	0.600000

in two main steps: first, we define a linear scaling limiter for each species to get positive solutions in each component and then we consider a second linear scaling limiter in such a way that the total concentration is bounded by $\phi_{\max}$. Finally, we apply a strong-stability preserving (SSP) third-order TVD Runge-Kutta time discretization to obtain the fully-discrete scheme. With this one can show that, under a more restrictive CFL condition, the resulting finite volume scheme is IRP and the high order of accuracy is not destroyed.

The numerical results obtained support the theoretical findings. In all the numerical simulations the minimum values of the solution for each species and the maximum value of the total concentration are computed and tabulated and the effect of the limiters is appreciated in both the tables and the plots of the solutions. As future perspectives, we wish to apply this strategy to multiclass vehicular dynamics with uneven space occupancy or with creeping, where some physical invariant regions different to $\mathcal{D}_{\phi_{\max}}$ are studied [57, 58]. Moreover, we intend to explore the extension of these modified scaling limiters to nonlocal two-dimensional multispecies models. On the other hand, we mention that multispecies kinematic flow models other than the MCLWR or MLB models could be handled by the present numerical method as well provided that the velocity functions $v_i(\Phi)$ have the properties outlined in Section 1.1. For instance, kinematic models of polydisperse sedimentation of the form (1.1) but with velocity functions $v_i(\Phi)$ alternative to the MLB model are discussed in [6, 15]. We also mention the model of gravity-driven separation of oil-water dispersions introduced in [7] whose velocity functions are equivalent to those of the MCLWR model but which is equipped with zero-flux boundary conditions.

Finally, we comment that there are no fundamentally difficulties in appying similar WENO schemes to two- or higher-dimensional systems of conservation laws that are multi-dimensional analogues of (1.1), for instance in two dimensions,

$$\partial_t \Phi + \partial_x \boldsymbol{f}^x(\Phi) + \partial_y \boldsymbol{f}^y(\Phi) = \boldsymbol{0}, \tag{6.1}$$
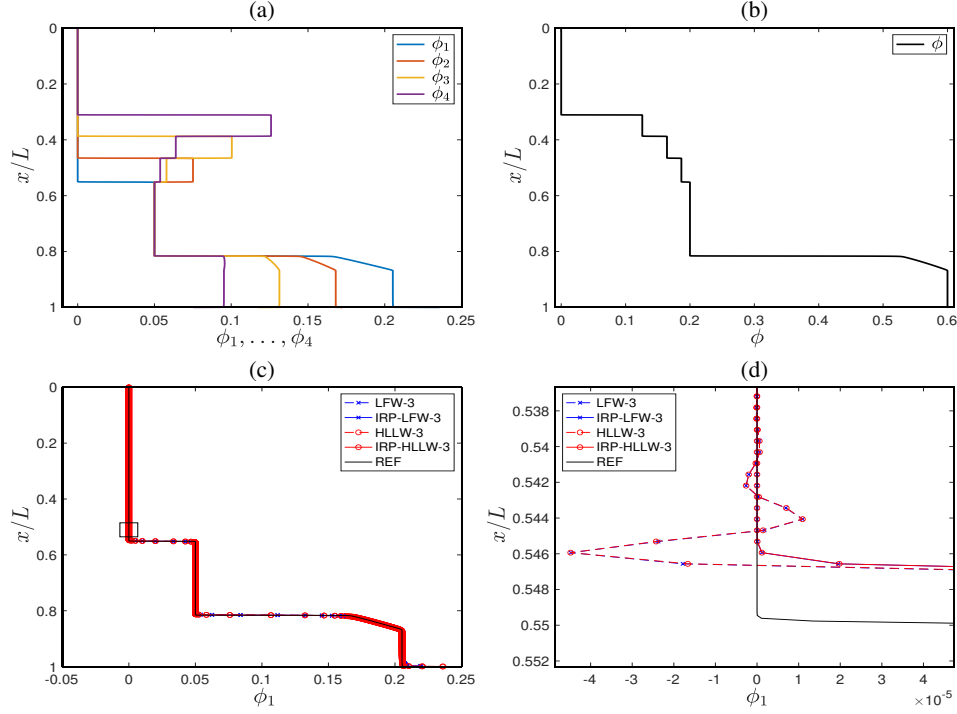
Figure 5: Example 3 (MLB model, $N = 4$): reference solution for (a) $\phi_1, \ldots, \phi_4$ and (b) ϕ at $T = 50\,\mathrm{s}$ computed by scheme IRP-HLLW-3 with $M_{\mathrm{ref}} = 6400$, and comparison of schemes for (c) ϕ_1, (d) enlarged view of (c) at $T = 50\,\mathrm{s}$ with $M = 1600$.

with functions $\boldsymbol{f}^x$ and $\boldsymbol{f}^y$ that have properties similar to those of $\boldsymbol{f}$ in (1.1), and in particular are compactly supported on $\mathcal{D}_{\phi_{\max}}$. However, models of polydisperse sedimentation require in two or more space dimensions the computation of a volume average flow field, which only in one space dimension is given by boundary conditions, and for the case of batch settling considered herein vanishes at all (cf., e.g., [4] for a complete formulation). That flow field gives rise to an additional advection term in the system of conservation laws governing the evolution of the concentration vector, and needs to be computed by a variant of the Stokes or Navier-Stokes equations. The flow is, moreover, driven by density fluctuations of the mixture, that is, by fluctuations of concentrations. Thus, the two-dimensional analogue of the MLB model is not just a multi-dimensional version of (1.1) but a coupled flow-transport problem, which is currently being investigated by the authors.

Acknowledgments

Appendix A. Interlacing property

Multispecies kinematic flow models are given by systems of conservation laws with fluxes as in (1.1) for sufficiently smooth functions v_i. However, in most applications, these functions do not depend individually on each of the
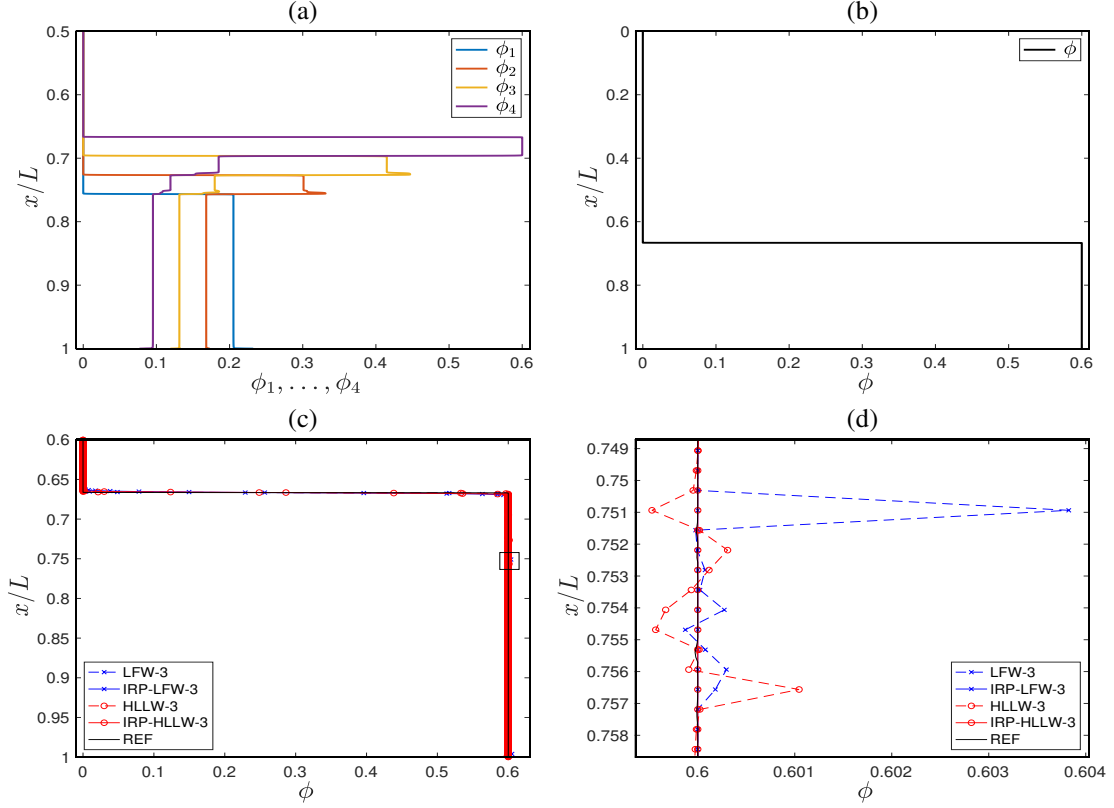
Figure 6: Example 3 (MLB model, $N = 4$): reference solution for (a) $\phi_1, \ldots, \phi_4$ and (b) ϕ at $T = 300\,\text{s}$ computed by scheme IRP-HLLW-3 with $M_{\text{ref}} = 6400$, and (c) comparison of schemes for ϕ, (d) enlarged view of (c) at $T = 300\,\text{s}$ with $M = 1600$.

densities $\phi_1, \ldots, \phi_N$ but rather on a small number $m \ll N$ of functions $p_1, \ldots, p_m$ of $\phi_1, \ldots, \phi_N$, as we presented in Section 2.2 and 2.1, i.e, we have

$$v_i = v_1(p_1, \ldots, p_m), \quad p_\ell = p_\ell(\phi_1, \ldots, \phi_N), \quad i = 1, \ldots, N, \quad \ell = 1, \ldots, m, \quad m \ll N.$$

Under this assumption we can write the Jacobian matrix $\mathcal{J}_f = \mathcal{J}_f(\Phi)$ in the form

$$\mathcal{J}_f = D + BC^{\text{T}}, \quad D := \text{diag}(v_1, \ldots, v_N), \tag{A.1}$$

$$B := (b_{i\ell}) = \left(\phi_i \frac{\partial v_i}{\partial p_\ell} \right), \quad C := (c_{j\ell}) = \left(\frac{\partial p_\ell}{\partial \phi_j} \right), \quad 1 \le i, j \le N, \quad 1 \le \ell \le m. \tag{A.2}$$

The following Theorem has been proved in [59] and it is used to show hyperbolicity of selected multispecies kinematic flow models and for the construction of spectral numerical schemes.

Theorem 4 (Secular equation [16, 59]). *Assume that D is a diagonal matrix as given by* (A.1) *with $v_i > v_j$ for $i < j$ and that C and B have the formats specified in* (A.2). *Let $\lambda \ne v_i$ for $i = 1, \ldots, N$. Then λ is an eigenvalue of $D + BC^{\text{T}}$ if and only if*

$$R(\lambda) := \det(M_\lambda) = 1 + \sum_{i=1}^{N} \frac{\gamma_i}{v_i - \lambda} = 0.$$

The coefficients $\gamma_1, \ldots, \gamma_N$ are given by the following expression, where $I := \{i_1 < \cdots < i_k\} \in S_k^N$ and $J := \{j_1 < \cdots <$

Table 5: Example 3 (MLB model, $N = 4$): L^1 errors, numerical order, and CPU time (seconds) for IRP-LFW-3 and IRP-HLLW-3 schemes at $T = 50\,\text{s}$ and $T = 300\,\text{s}$. The reference solution is computed by IRP-HLLW-3 with $M_{\text{ref}} = 6400$.

M	e_M^{tot}	θ_M	cpu [s]	e_M^{tot}	θ_M	cpu [s]	e_M^{tot}	θ_M	cpu [s]	e_M^{tot}	θ_M	cpu [s]
	IRP-LFW-3, $T = 50\,\text{s}$			IRP-LFW-3, $T = 300\,\text{s}$			IRP-HLLW-3, $T = 50\,\text{s}$			IRP-HLLW-3, $T = 300\,\text{s}$		
100	6.89e-03	—	5.24e-02	1.83e-03	—	1.75e-01	5.60e-03	—	8.17e-02	1.75e-03	—	3.09e-01
200	3.54e-03	0.9	1.04e-01	1.15e-03	0.7	5.37e-01	2.86e-03	1.0	1.94e-01	6.69e-04	1.4	1.03
400	1.93e-03	0.8	4.11e-01	6.07e-04	0.9	2.15	1.54e-03	0.9	7.88e-01	3.36e-04	0.9	4.29
800	1.05e-03	0.8	1.61	2.82e-04	1.1	8.59	8.48e-04	0.8	3.21	1.64e-04	1.1	16.6
1600	4.87e-04	1.1	6.31	1.29e-04	1.1	33.6	3.78e-04	1.1	12.8	9.00e-05	0.8	67.6

Table 6: Example 3 (MLB model, $N = 4$): minimum of the solutions $\phi_{i,j}^n$, $i = 1, \ldots, 4$, and maximum of the solution ϕ_j^n obtained by schemes LFW-3 (without limiters) and IRP-LFW-3 (with limiters) until specified times T.

M	$\underline{\phi}_{\cdot,1}$	$\underline{\phi}_{\cdot,2}$	$\underline{\phi}_{\cdot,3}$	$\underline{\phi}_{\cdot,4}$	$\overline{\phi}$	$\underline{\phi}_{\cdot,1}$	$\underline{\phi}_{\cdot,2}$	$\underline{\phi}_{\cdot,3}$	$\underline{\phi}_{\cdot,4}$	$\overline{\phi}$
	LFW-3, $T = 50\,\text{s}$					IRP-LFW-3, $T = 50\,\text{s}$				
100	-6.109e-004	-5.443e-004	-4.791e-004	-4.305e-004	0.599930	8.428e-058	1.248e-024	2.774e-014	6.634e-08	0.598892
200	-3.687e-004	-3.199e-004	-2.806e-004	-2.157e-004	0.604964	2.437e-118	1.606e-047	1.825e-026	2.213e-013	0.599973
400	-1.845e-004	-1.598e-004	-1.401e-004	-1.080e-004	0.607519	1.817e-239	3.064e-093	7.809e-051	3.408e-024	0.600000
800	-9.229e-005	-7.978e-005	-6.993e-005	-5.411e-005	0.609175	1.828e-322	1.303e-184	1.687e-099	1.232e-045	0.600000
1600	-4.610e-005	-3.983e-005	-3.491e-005	-2.709e-005	0.605247	1.976e-322	3.112e-322	1.033e-196	2.660e-088	0.600000
	LFW-3, $T = 300\,\text{s}$					IRP-LFW-3, $T = 300\,\text{s}$				
100	-8.523e-004	-6.713e-004	-5.662e-004	-4.305e-004	0.666358	1.172e-203	5.930e-064	5.930e-041	1.990e-025	0.600000
200	-3.908e-004	-3.403e-004	-2.806e-004	-2.157e-004	0.609710	2.173e-322	8.387e-128	3.934e-081	7.523e-050	0.600000
400	-2.070e-004	-1.701e-004	-1.401e-004	-1.080e-004	0.628049	2.025e-322	9.918e-256	1.585e-161	9.329e-099	0.600000
800	-1.376e-004	-1.329e-004	-1.314e-004	-5.411e-005	0.649020	1.729e-322	3.112e-322	6.175e-322	1.184e-196	0.600000
1600	-5.020e-004	-5.744e-005	-5.204e-005	-2.709e-005	0.605247	1.877e-322	3.013e-322	4.199e-322	6.472e-322	0.600000

$j_\ell\} \in S_\ell^m$ are index sets:

$$\gamma_i = \sum_{r=1}^{\min\{N,m\}} \sum_{i \in S_r^N, J \in S_r^m} \frac{\det \boldsymbol{C}^{I,J}}{\prod_{\ell \in I, \ell \neq i}(v_\ell - v_i)}.$$

Corollary 1 (Interlacing property [6])**.** *With the notation of the theorem above, assume that $\gamma_i\gamma_j > 0$ for $i, j = 1, \ldots, N$. Then $\boldsymbol{D} + \boldsymbol{BC}^{\mathrm{T}}$ is diagonalizable with real eigenvalues $\lambda_1, \ldots, \lambda_N$. If $\gamma_1, \ldots, \gamma_N < 0$, the interlacing property*

$$M_1 := v_N + \gamma_1 + \cdots + \gamma_N < \lambda_N < v_N < \lambda_{N-1} < \cdots < \lambda_1 < v_1 \tag{A.3}$$

holds, while for $\gamma_1, \ldots, \gamma_N > 0$, the following analogous property holds:

$$v_N < \lambda_N < v_{N-1} < \lambda_{N-1} < \cdots < v_1 < \lambda_1 < M_2 := v_1 + \gamma_1 + \cdots + \gamma_N. \tag{A.4}$$

Remark 5. *Theorem 4 and Corollary 1 apply to the MCLWR and MLB models (see (2.2) and (2.8)) for the respective specific bounds).*

References

[1] G. C. K. Wong, S. C. Wong, A multi-class traffic flow model–an extension of LWR model with heterogeneous drivers, Transp. Res. A 36 (2002) 827–841.

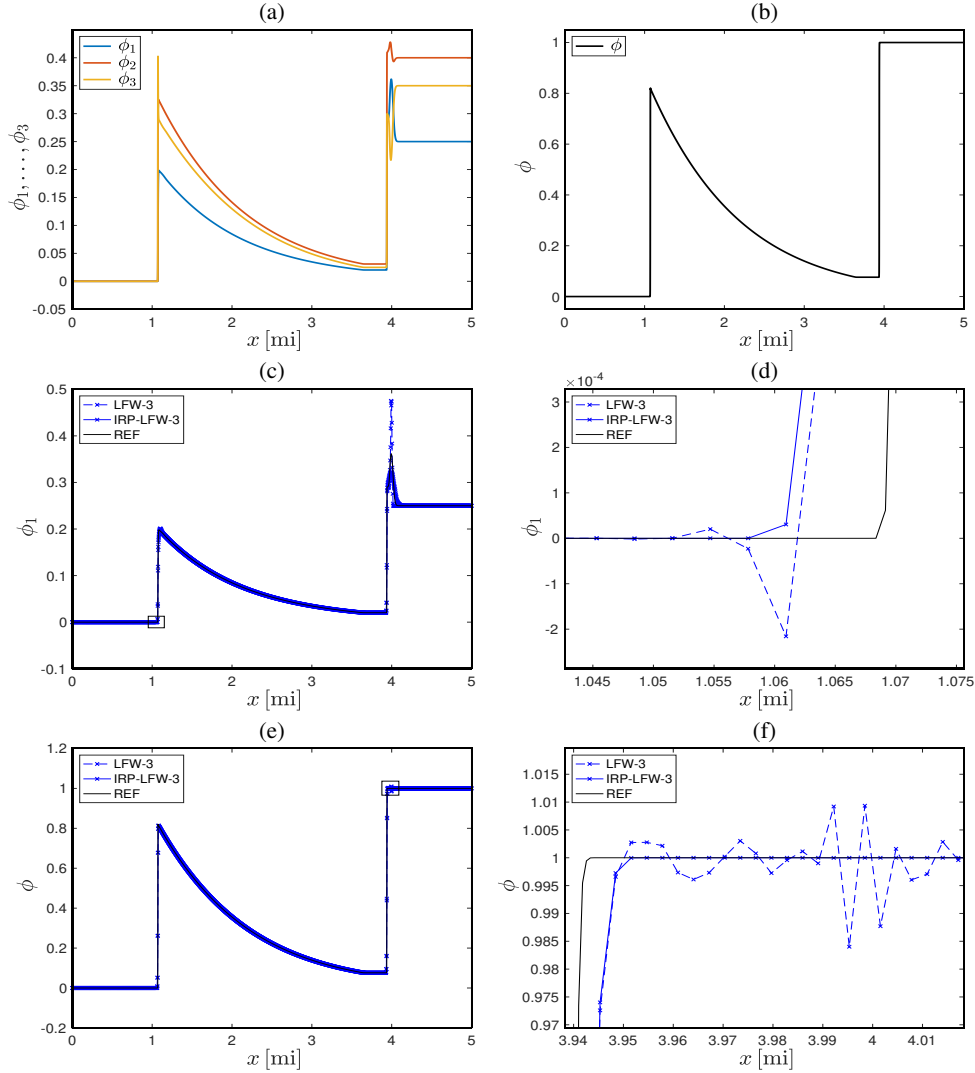[2] S. Benzoni-Gavage, R. M. Colombo, An-populations model for traffic flow, Eur. J. Appl. Math. 14 (2003) 587–612.

Figure 7: Example 4 (MCLWR model, $N = 3$): reference solution for (a) ϕ_1, ϕ_2, ϕ_3 and (b) ϕ at $T = 0.05\,\text{h}$ computed by scheme IRP-HLLW-3 with $M_{\text{ref}} = 6400$, and comparison of schemes for (c) ϕ_3, (d) enlarged view of (c), (e) ϕ, and (f) enlarged view of (e) at $T = 0.05\,\text{h}$ with $M = 1600$.

[3] R. Bürger, F. Concha, K.-K. Fjelde, K. H. Karlsen, Numerical simulation of the settling of polydisperse suspensions of spheres, Powder Technol. 113 (2000) 30–54.

[4] R. Bürger, K. H. Karlsen, E. M. Tory, W. L. Wendland, Model equations and instability regions for the sedimentation of polydisperse suspensions of spheres, ZAMM Z. Angew. Math. Mech. 82 (2002) 699–722.

[5] S. Berres, R. Bürger, E. M. Tory, Applications of polydisperse sedimentation models, Chem. Eng. J. 111 (2005) 105–117.

[6] R. Bürger, R. Donat, P. Mulet, C. A. Vega, Hyperbolicity analysis of polydisperse sedimentation models via a secular equation for the flux Jacobian, SIAM J. Appl. Math. 70 (2010) 2186–2213.

[7] F. Rosso, G. Sona, Gravity-driven separation of oil-water dispersions, Adv. Math. Sci. Appl. 11 (2001) 127–151.

[8] X. Zhang, C.-W. Shu, On maximum-principle-satisfying high order schemes for scalar conservation laws, J. Comput. Phys. 229 (2010) 3091–3120.

[9] S. Gottlieb, C.-W. Shu, E. Tadmor, Strong stability-preserving high-order time discretization methods, SIAM review 43 (1) (2001) 89–112.

[10] S. Gottlieb, D. I. Ketcheson, C.-W. Shu, High order strong stability preserving time discretizations, J. Sci. Comput. 38 (2009) 251–289.

[11] H. Frid, Invariant regions under Lax-Friedrichs scheme for multidimensional systems of conservation laws, Discr. Cont. Dyn. Syst. 1 (1995) 585–593.

[12] R. Bürger, A. García, K. H. Karlsen, J. D. Towers, A family of numerical schemes for kinematic flows with discontinuous flux, J. Engrg. Math. 60 (2008) 387–425.

[13] R. Bürger, C. Chalons, L. M. Villada, Antidiffusive and random-sampling Lagrangian-remap schemes for the multiclass Lighthill-Whitham-
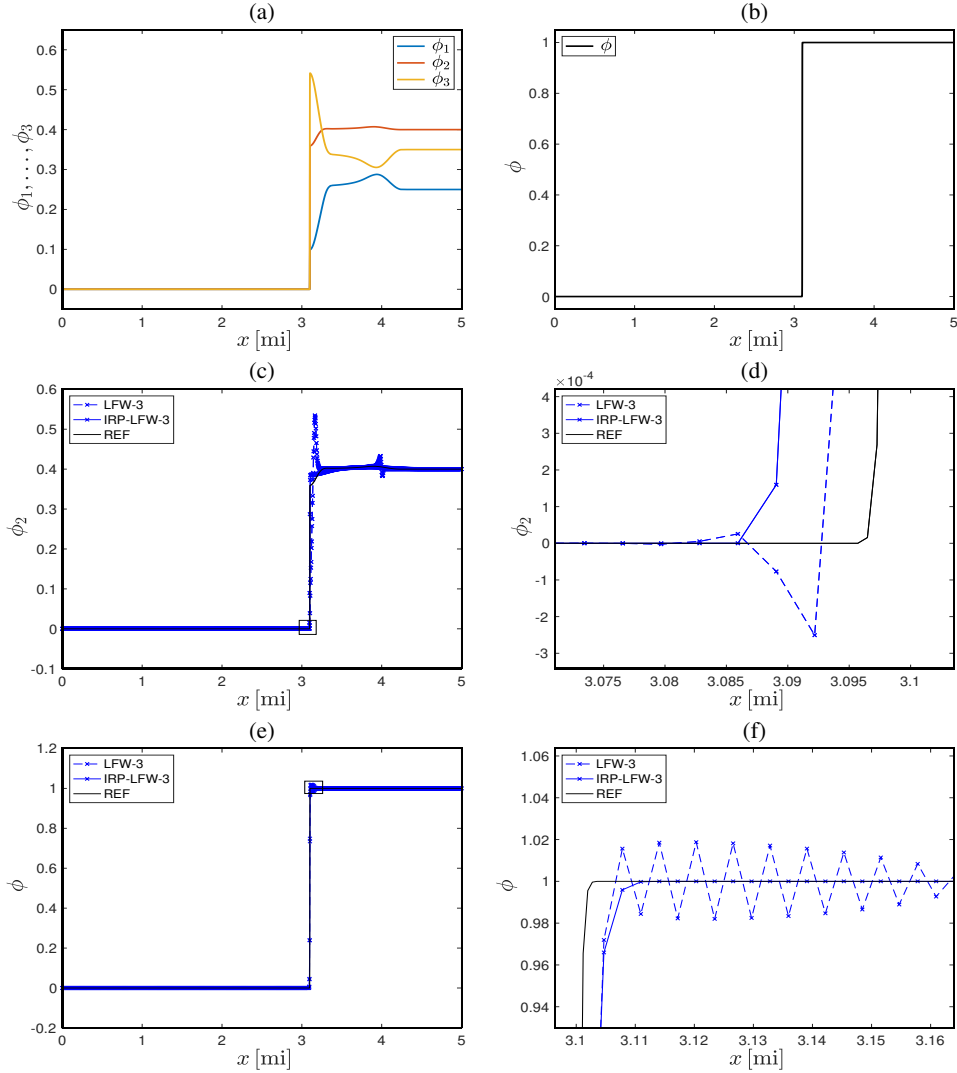
Figure 8: Example 4 (MCLWR model, $N = 3$): reference solution for (a) ϕ_1, ϕ_2, ϕ_3 and (b) ϕ at $T = 0.5\,\mathrm{h}$ computed by scheme IRP-HLLW-3 with $M_{\mathrm{ref}} = 6400$, and comparison of schemes for (c) ϕ_2, (d) enlarged view of (c), (e) ϕ, and (f) enlarged view of (e) at $T = 0.5\,\mathrm{h}$ with $M = 1600$.

Richards traffic model, SIAM J. Sci. Comput. 35 (2013) B1341–B1368.

[14] R. Bürger, A. Kozakevicius, Adaptive multiresolution WENO schemes for multi-species kinematic flow models, J. Comput. Phys. 224 (2007) 1190–1222.

[15] R. Bürger, R. Donat, P. Mulet, C. A. Vega, On the implementation of WENO schemes for a class of polydisperse sedimentation models, J. Comput. Phys. 230 (2011) 2322–2344.

[16] R. Donat, P. Mulet, A secular equation for the Jacobian matrix of certain multispecies kinematic flow models, Numer. Meth. Partial Diff. Eqns. 26 (2010) 159–175.

[17] R. Bürger, P. Mulet, L. M. Villada, Spectral WENO schemes with adaptive mesh refinement for models of polydisperse sedimentation, ZAMM Z. Angew. Math. Mech. 93 (2013) 373–386.

[18] R. Bürger, P. Mulet, L. Rubio, Polynomial viscosity methods for multispecies kinematic flow models, Numer. Meth. Partial Diff. Eqns. 32 (2016) 1265–1288.

[19] R. Bürger, H. Torres, C. A. Vega, An entropy stable scheme for the multiclass Lighthill-Whitham-Richards traffic model, Adv. Appl. Math. Mech 11 (2019) 1022–1047.

[20] X. Zhang, C.-W. Shu, On positivity-preserving high order discontinuous Galerkin schemes for compressible Euler equations on rectangular meshes, J. Comput. Phys. 229 (2010) 8918–8934.

[21] X. Zhang, C.-W. Shu, Maximum-principle-satisfying and positivity-preserving high-order schemes for conservation laws: survey and new developments, Proc. Roy. Soc. A 467 (2134) (2011) 2752–2776.

Table 7: Example 4 (MCLWR model, $N = 3$): L^1 errors, numerical order, and CPU time (seconds) for scheme IRP-LFW-3 at $T = 0.05\,\text{h}$ and $T = 0.5\,\text{h}$. The reference solution is computed by IRP-LFW-3 with $M_{\text{ref}} = 6400$.

M	e_M^{tot}	θ_M	cpu [s]	e_M^{tot}	θ_M	cpu [s]
	IRP-LFW-3, $T = 0.05\,\text{h}$			IRP-LFW-3, $T = 0.5\,\text{h}$		
100	7.45e-03	—	9.67e-03	4.99e-03	—	9.77e-02
200	3.51e-03	1.1	2.96e-02	2.67e-03	0.9	2.26e-01
400	1.87e-03	0.9	1.02e-01	1.32e-03	1.0	1.05
800	8.03e-04	1.2	4.23e-01	6.26e-04	1.0	4.07
1600	4.04e-04	1.0	1.6	2.70e-04	1.2	16.2

Table 8: Example 4 (MCLWR model, $N = 3$): minimum of the solutions $\phi_{i,j}^n$, $i = 1, \ldots, 3$, and maximum of the solution ϕ_j^n obtained by schemes LFW-3 (without limiters) and IRP-LFW-3 (with limiters) until specified times T.

M	$\underline{\phi}_{,1}$	$\underline{\phi}_{,2}$	$\underline{\phi}_{,3}$	$\overline{\phi}$	$\underline{\phi}_{,1}$	$\underline{\phi}_{,2}$	$\underline{\phi}_{,3}$	$\overline{\phi}$
	LFW-3, $T = 0.05\,\text{h}$				IRP-LFW-3, $T = 0.05\,\text{h}$			
100	-4.580e-03	-4.976e-03	-4.914e-03	1.01102	0.00000	0.00000	0.00000	1.00000
200	-2.744e-03	-3.031e-03	-2.636e-03	1.01537	0.00000	0.00000	0.00000	1.00000
400	-1.759e-03	-1.934e-03	-1.891e-03	1.04909	0.00000	0.00000	0.00000	1.00000
800	-1.117e-03	-1.531e-03	-1.344e-03	1.05402	0.00000	0.00000	0.00000	1.00000
1600	-9.064e-04	-1.058e-03	-9.975e-04	1.06708	0.00000	0.00000	0.00000	1.00000
	LFW-3, $T = 0.5\,\text{h}$				IRP-LFW-3, $T = 0.5\,\text{h}$			
100	-5.041e-03	-5.887e-03	-7.050e-03	1.04260	0.00000	0.00000	0.00000	1.00000
200	-3.446e-03	-3.031e-03	-3.518e-03	1.07077	0.00000	0.00000	0.00000	1.00000
400	-2.447e-03	-2.711e-03	-1.891e-03	1.06805	0.00000	0.00000	0.00000	1.00000
800	-2.137e-03	-2.499e-03	-1.344e-03	1.09395	0.00000	0.00000	0.00000	1.00000
1600	-1.779e-03	-1.225e-03	-9.975e-04	1.09029	0.00000	0.00000	0.00000	1.00000

[22] D. Levy, G. Puppo, G. Russo, Central WENO schemes for hyperbolic systems of conservation laws, ESAIM: Math. Model. Numer. Anal. 33 (1999) 547–571.

[23] G.-S. Jiang, C.-W. Shu, Efficient implementation of weighted ENO schemes, J. Comput. Phys. 126 (1996) 202–228.

[24] J. Zhu, C.-W. Shu, A new type of multi-resolution WENO schemes with increasingly higher order of accuracy, J. Comput. Phys. 375 (2018) 659–683.

[25] R. Borges, M. Carmona, B. Costa, W. S. Don, An improved weighted essentially non-oscillatory scheme for hyperbolic conservation laws, J. Comput. Phys. 227 (2008) 3191–3211.

[26] T. Arbogast, C.-S. Huang, X. Zhao, Accuracy of WENO and adaptive order WENO reconstructions for solving conservation laws, SIAM J. Numer. Anal. 56 (3) (2018) 1818–1847. doi:10.1137/17M1154758.

[27] A. Harten, P. D. Lax, B. van Leer, On upstream differencing and Godunov-type schemes for hyperbolic conservation laws, SIAM Rev. 25 (1983) 35–61.

[28] M. Hilliges, W. Weidlich, A phenomenological model for dynamic traffic flow in networks, Transp. Res. B 29 (1995) 407–431.

[29] S. Jaouen, F. Lagoutière, Numerical transport of an arbitrary number of components, Comput. Meth. Appl. Mech. Engrg. 196 (2007) 3127–3140.

[30] M. Ancellin, B. Després, S. Jaouen, Extension of generic two-component VOF interface advection schemes to an arbitrary number of components, J. Comput. Phys. 473 (2023) 111721.

[31] A. Baumgart, G. Blanquart, Ensuring $\sum_s y_s = 1$ in transport of species mass fractions, J. Comput. Phys. (2024) 113199.

[32] Z. Huang, E. Johnsen, A consistent and conservative phase-field method for compressible N-phase flows: Consistent limiter and multiphase reduction-consistent formulation, J. Comput. Phys. 501 (2024) 112801.

[33] X. Zhang, C.-W. Shu, Positivity-preserving high order discontinuous Galerkin schemes for compressible Euler equations with source terms, J. Comput. Phys. 230 (2011) 1238–1248.

[34] W. Zhang, Y. Xing, Y. Xia, Y. Xu, High-order positivity-preserving well-balanced discontinuous Galerkin methods for Euler equations with gravitation on unstructured meshes, Commun. Comput. Phys. 31 (2022) 771–815.

[35] Y. Xing, X. Zhang, C.-W. Shu, Positivity-preserving high order well-balanced discontinuous Galerkin methods for the shallow water equations, Adv. Wat. Res. 33 (2010) 1476–1493.

[36] Y. Xing, X. Zhang, Positivity-preserving well-balanced discontinuous Galerkin methods for the shallow water equations on unstructured
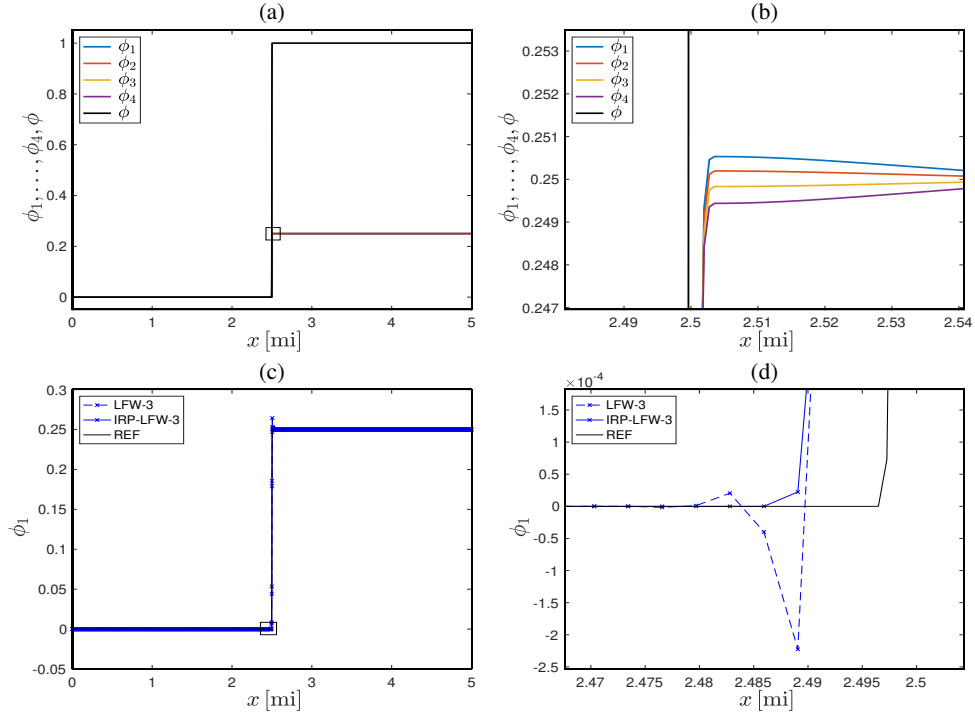
Figure 9: Example 5 (MCLWR model, Daganzo's test, $N = 4$): reference solution for (a) $\phi_1, \ldots, \phi_4$ and ϕ, (b) enlarged view of (a) at $T = 0.5$ h computed by scheme IRP-HLLW-3 with $M_{\mathrm{ref}} = 6400$, and comparison of schemes for (c) ϕ_1, (d) enlarged view of (c), (e) ϕ, and (f) enlarged view of (e) at $T = 0.5$ h with $M = 1600$.

triangular meshes, J. Sci. Comput. 57 (2013) 19–41.

[37] D. Kuzmin, H. Hajduk, Property-preserving numerical schemes for conservation laws, World Scientific, 2024.

[38] M. J. Lighthill, G. B. Whitham, On kinematic waves. II. A theory of traffic flow on long crowded roads, Proc. Roy. Soc. London Ser. A 229 (1955) 317–345.

[39] P. I. Richards, Shock waves on the highway, Operations Res. 4 (1956) 42–51.

[40] X. Zhang, On positivity-preserving high order discontinuous galerkin schemes for compressible navier–stokes equations, Journal of Computational Physics 328 (2017) 301–343.

[41] B. D. Greenshields, J. R. Bibbins, W. S. Channing, H. H. Miller, A study of traffic capacity, in: Highway Research Board Proceedings, Vol. 14, Washington, DC, 1935, pp. 448–477.

[42] A. C. Dick, Speed/flow relationships within an urban area, Traffic Eng. Control 8 (6) (1966) 393–396.

[43] H. Greenberg, An analysis of traffic flow, Operations Research 7 (1) (1959) 79–85.

[44] R. Donat, P. Mulet, Characteristic-based schemes for multi-class Lighthill-Whitham-Richards traffic models, J. Sci. Comput. 37 (2008) 233–250.

[45] P. Zhang, R.-X. Liu, S. C. Wong, S.-Q. Dai, Hyperbolicity and kinematic waves of a class of multi-population partial differential equations, European J. Appl. Math. 17 (2006) 171–200.

[46] J. H. Masliyah, Hindered settling in a multi-species particle system, Chem. Eng. Sci. 34 (1979) 1166–1168.

[47] M. J. Lockett, K. S. Bassoon, Sedimentation of binary particle mixtures, Powder Technol. 24 (1979) 1–7.

[48] J. F. Richardson, W. N. Zaki, Sedimentation and fluidization I, Trans. Instn. Chem. Engrs. (London) 32 (1954) 35–53.

[49] X.-D. Liu, S. Osher, T. Chan, Weighted essentially non-oscillatory schemes, J. Comput. Phys. 115 (1994) 200–212.

[50] D. Levy, G. Puppo, G. Russo, Compact central WENO schemes for multidimensional conservation laws, SIAM J. Sci. Comput. 22 (2000) 656–672.

[51] I. Cravero, G. Puppo, M. Semplice, G. Visconti, CWENO: uniformly accurate reconstructions for balance laws, Math. Comp. 87 (2018) 1689–1719.

[52] S. Boscarino, R. Bürger, P. Mulet, G. Russo, L. M. Villada, On linearly implicit IMEX Runge-Kutta methods for degenerate convection-diffusion problems modeling polydisperse sedimentation, Bull. Braz. Math. Soc. (N.S.) 47 (2016) 171–185.

[53] W. Schneider, G. Anestis, U. Schaflinger, Sediment composition due to settling of particles of different sizes, Int. J. Multiphase Flow 11 (1985) 419–423.

[54] H. P. Greenspan, M. Ungarish, On hindered settling of particles of different sizes, Int. J. Multiphase Flow 8 (1982) 587–604.

[55] R. Bürger, W. L. Wendland, F. Concha, Model equations for gravitational sedimentation-consolidation processes, ZAMM Z. Angew. Math. Mech. 80 (2000) 79–92.

Table 9: Example 5 (MCLWR model, Daganzo's test, $N = 4$): minimum of the solutions $\phi_{i,j}^n$, $i = 1, \ldots, 4$, and maximum of the solution ϕ_j^n obtained by schemes LFW-3 (without limiters) and IRP-LFW-3 (with limiters) until a specified time T.

M	$\underline{\phi}_{,1}$	$\underline{\phi}_{,2}$	$\underline{\phi}_{,3}$	$\underline{\phi}_{,4}$	$\overline{\phi}$	$\underline{\phi}_{,1}$	$\underline{\phi}_{,2}$	$\underline{\phi}_{,3}$	$\underline{\phi}_{,4}$	$\overline{\phi}$
	LFW-3, $T = 0.5\,\text{h}$					IRP-LFW-3, $T = 0.5\,\text{h}$				
100	-2.186e-003	-2.673e-003	-3.177e-003	-3.691e-003	1.00403	0.00000	0.00000	0.00000	0.00000	1.00000
200	-1.832e-003	-1.938e-003	-1.987e-003	-1.953e-003	1.01107	0.00000	0.00000	0.00000	0.00000	1.00000
400	-9.020e-004	-6.778e-004	-6.999e-004	-8.780e-004	1.00369	0.00000	0.00000	0.00000	0.00000	1.00000
800	-3.076e-004	-3.848e-004	-4.523e-004	-4.882e-004	1.00107	0.00000	0.00000	0.00000	0.00000	1.00000
1600	-2.266e-004	-2.356e-004	-2.084e-004	-1.960e-004	1.00122	0.00000	0.00000	0.00000	0.00000	1.00000

[56] C. F. Daganzo, Requiem for second-order fluid approximations of traffic flow, Transp. Res. B 29 (1995) 277–286.

[57] M. Briani, E. Cristiani, P. Ranut, Macroscopic and multi-scale models for multi-class vehicular dynamics with uneven space occupancy: a case study, Axioms 10 (2) (2021) 102.

[58] S. Fan, D. B. Work, A heterogeneous multiclass traffic flow model with creeping, SIAM J. Appl. Math. 75 (2015) 813–835.

[59] J. Anderson, A secular equation for the eigenvalues of a diagonal matrix perturbation, Linear Algebra Appl. 246 (1996) 49–70.